journal homepage: www.intl.elsevierhealth.com/journals/cmpb

A review of atlas-based segmentation for magnetic resonance brain images

Mariano Cabezas[a,c], *Arnau Oliver*[a,*], *Xavier Lladó*[a], *Jordi Freixenet*[a], *Meritxell Bach Cuadra*[b,c]

[a] *Institute of Informatics and Applications, Ed. P-IV, Campus Montilivi, University of Girona, 17071 Girona, Spain*
[b] *Department of Radiology, University Hospital Center and University of Lausanne, Switzerland*
[c] *Signal Processing Laboratory (LTS5), École Polytechnique Fédérale de Lausanne, Switzerland*

ARTICLE INFO

Article history:
Received 20 May 2010
Received in revised form
26 July 2011
Accepted 27 July 2011

Keywords:
Atlas
Segmentation
Magnetic resonance imaging
Brain
Automated methods

ABSTRACT

Normal and abnormal brains can be segmented by registering the target image with an atlas. Here, an atlas is defined as the combination of an intensity image (template) and its segmented image (the atlas labels). After registering the atlas template and the target image, the atlas labels are propagated to the target image. We define this process as atlas-based segmentation. In recent years, researchers have investigated registration algorithms to match atlases to query subjects and also strategies for atlas construction. In this paper we present a review of the automated approaches for atlas-based segmentation of magnetic resonance brain images. We aim to point out the strengths and weaknesses of atlas-based methods and suggest new research directions. We use two different criteria to present the methods. First, we refer to the algorithms according to their atlas-based *strategy*: label propagation, multi-atlas methods, and probabilistic techniques. Subsequently, we classify the methods according to their *medical target*: the brain and its internal structures, tissue segmentation in healthy subjects, tissue segmentation in fetus, neonates and elderly subjects, and segmentation of damaged brains. A quantitative comparison of the results reported in the literature is also presented.

1. Introduction

Magnetic resonance imaging (MRI) of the brain is widely used in clinical practice for diagnosis [1], patient follow-up [2], therapy evaluation [3] and human brain mapping [4]. This is due to it being non-invasive, its good spatial resolution and fast acquisition, and its excellent performance when visualising differences in various human body tissues. However, despite the large number of segmentation methods published in scientific journals, the use of semi-automated and automated tools is relatively limited in clinical practice. This can be explained by the difficulty of quantitatively validating these tools and adapting them to large databases (with images from different scanners or different sequences).

The automated segmentation of MR brain images is a challenging task due to image artifacts (such as intensity inhomogeneities and partial volume effects) and due to the fact that different anatomical structures may share the same tissue contrast. Hence, *a priori* anatomical information is essential for simplifying the segmentation task. Prior information may be provided in different ways, for instance, as a set of predefined rules based on known tissue properties, or as a set of manual expert annotations. In this study, we focus

* *Corresponding author*. Tel.: +34 972418878; fax: +34 972 418259.
E-mail address: aoliver@eia.udg.edu (A. Oliver).
0169-2607/$ – see front matter © 2011 Elsevier Ireland Ltd. All rights reserved.
doi:10.1016/j.cmpb.2011.07.015

on anatomical priors from an atlas to be matched to the target volume we wish to segment. Here, we consider an atlas as two image volumes: one intensity image (or *template*) and one segmented image (or *labelled* image). Note however that, as stated in [5], active shape models [6] or active appearance models [7] can also be considered as atlases since they bring spatial prior knowledge to the segmentation process.

At this point, the segmentation turns into a registration problem. Volumetric registration is often done in two steps. Firstly, a global registration (affine or rigid transformation) is performed to obtain an initial alignment at a low computational cost. Secondly, a local registration is applied to adapt general models to a specific anatomy. Note that this local registration provides a better match between different brains at the expense of a high computational cost. Multi-resolution strategies may be used to reduce this computational cost [8].

Medical image registration has been widely reviewed in the literature [9–13]. These studies include reviews of registration techniques that can be used to align an atlas to an unseen MRI scan. However, to the best of our knowledge, our study is the first attempt to review the use of atlases for automatic segmentation of brain structures and tissues. In particular, we first distinguish between three different ways of integrating the atlas information into the whole segmentation process: *label propagation*, *multi-atlas propagation* and *probabilistic atlas-based segmentation*. We then go on to review the atlas-based segmentation methods according to their medical target: those that segment the brain and its internal structures (such as the amygdala or putamen), those that target brain tissues in healthy brains, those that target brain tissues in fetus, neonates and elderly subjects, and, finally, those that segment damaged brains with either focal lesions (such as multiple sclerosis lesions) or space-occupying lesions (like tumours).

For comparison purposes, atlas-based segmentation methods should be applied to a common database and quantitatively validated using ground truth. Unfortunately, only very few of such methods and databases are publicly available. Atlas-based segmentation methods also aim to segment different targets, such as, for instance, brain structures, brain tissues, or lesions. Our contribution is closely related to this idea, comparing atlas-based segmentation approaches qualitatively and quantitatively according to their strategy, target and accuracy reported in the literature.

The rest of this paper is organised as follows. In Section 2, we introduce the different types of public atlases, also describing their creation process. Then, in Section 3, we present the strategies used to integrate atlases into the segmentation process. In Section 4 we analyse and classify the reviewed methods according to the ultimate objectives of segmentation. Finally, future trends are suggested in Section 5.

2. Type of brain atlases

The construction of a realistic anatomical brain atlas is a time-consuming task, especially when aimed at describing human data variability. Public atlas repositories have been created to provide the research community with MRI data to go with the manual segmentations (or annotations) performed by expert radiologists. The contribution of these repositories is twofold: firstly, they allow the training of new segmentation algorithms, and secondly they allow evaluation data to be standardised for the developed algorithms.

2.1. Topological atlases

First attempts at atlas construction of the human brain were based on a single subject. In the literature these atlases are called *topological*, *single-subject* or *deterministic* atlases. The single-subject atlas is often a volume image that has been selected from a data set to be representative of the objects to be segmented in other images (average size, shapes or intensity).

In medicine, pioneering work was done with the Talairach atlas [14,15], which was proposed to identify deep brain structures in stereotaxic coordinates. One of the first deterministic digital atlases was provided by the Visible Human Project of the National Library of Medicine [16]. The goal of this project was to create complete and detailed three-dimensional anatomical representations of normal male and female human bodies. These representations were obtained through the acquisition of transverse Computed Tomography (CT), MR and high-resolution cryosection images of male and female cadavers. Also derived from a digitised cryosectioned human brain, the Karolinska Institute and Hospital, Stockholm, created a Computerised Brain Atlas (CBA) that was designed for display and analysis of tomographic brain images. The atlas includes the brain surface, the ventricular system and about 400 structures and all Brodmann areas [17,18].

Nowadays, the vast majority of deterministic atlases are generated from imaging acquisition. For instance, the Surgical Planning Laboratory's (SPL) digital brain atlas, developed by the Harvard Medical School [19], is based on a 3D MR atlas of the human brain to visualise spatially complex structures. For CT acquisitions, Bajcsy et al. [20,21] created an artificial CT anatomical atlas based on the stained slices of a dead soldier's brain belonging to a 31 year-old normal male (from the so-called Yakovlev Collection). The McConell Brain Imaging Center [22] provides the research community with a digital brain phantom, based on 27 high-resolution scans from the same individual. Its average resulted in a high-resolution (1 mm isotropic voxels) brain atlas with an increased signal-to-noise ratio. This brain template is the reference data in the *BrainWeb* Simulated Brain Database [23]. Recently, 20 new normal anatomical models have become available as well as an anatomical model of a brain with Multiple Sclerosis (MS) lesions.

2.2. Probabilistic atlases

Atlases based on a single-subject are not constructed to represent the diversity of human anatomy. To better characterise the variability of anatomical structures, atlases have been constructed on the basis of populations. These atlases are often cited as *population-based*, *statistical* or *probabilistic* atlases. Such templates are in continuous evolution, as new images can easily be incorporated. Moreover, the population represented by a probabilistic atlas can be easily subdivided into groups according to specific criteria (age, sex, handedness, etc.). As for single-subject atlases, the first population-based atlases

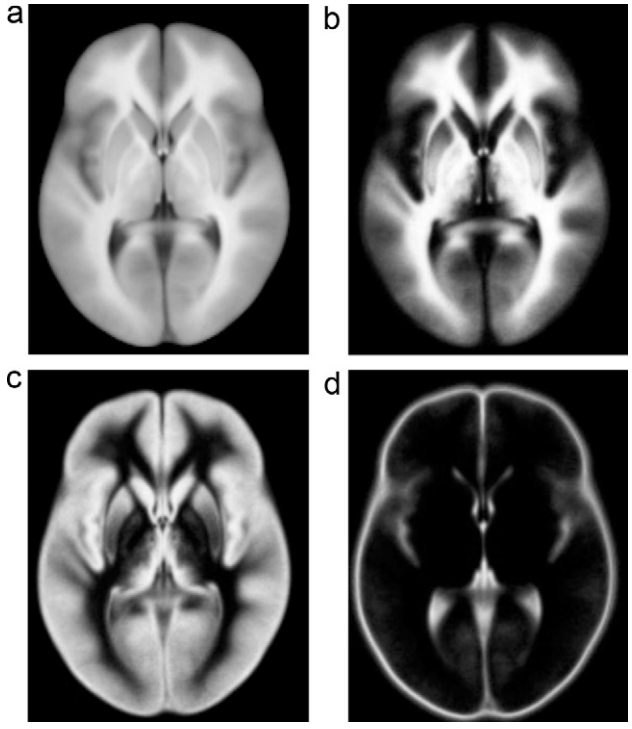

Fig. 1 – ICBM452 population-based atlas [27]: (a) T1-weighted mean, (b) white matter, (c) grey matter, and (d) cerebrospinal fluid.

were based in Talairach space [24,25]. Later, to compensate for the implicit limitations of Talairach space, such as poor resolution across slices (from 3 to 4 mm), population-based atlases from MR images were proposed. A composite MRI data set was constructed by Evans et al. [26] from several hundreds of normal subjects (239 males and 66 females of 23.4 ± 4.1 years old). All the scans were first individually registered in the Talairach coordinate system. Following this they were intensity normalised and, finally all the scans were averaged voxel-by-voxel and probabilistic maps for brain tissue were created. The same procedure for constructing an average brain was later used by the International Consortium for Brain Mapping (ICBM) on 152 brains and later on 452 brains [27]. Fig. 1 shows the tissue probabilities for one central slice of the ICBM452 template. The UCLA Laboratory Of Neuro Imaging (LONI), which is a member of the ICBM, provides also atlases for MR brain imaging contrasts, such as T2-weighted or Diffusion Tensor Imaging (DTI) [28].

Another widely used repository for MRI brain data is the Internet Brain Segmentation Repository (IBSR) [29]. The MRI studies contained in this database have also been used either to define a set of topological atlases for multi-atlas strategies (using the included manual segmentations) or to construct a probabilistic atlas after co-registering all the segmented cases to a standard space and computing the frequency of each voxel to belong to a specific structure [30,31].

Interest in disease-based atlas construction [32,33] has increased in recent years. For instance, the ICBM provides an Alzheimer's disease template. Disease atlases allow quantitative examination of the history and evolution (due to natural disease evolution or reaction to clinical treatment) of a specific disease.

Important questions arise when generating population-based atlases, such as selecting a reference space or the registration method for the data alignment. Many researchers have proposed new strategies to create unbiased average templates and multi-subject registration [34–41].

3. Segmentation strategies

In formulating atlas-based segmentation, we can define the input image to be segmented, $I(x)$, as $I : x \in \mathbb{R}^3 \mapsto I(x) \in \mathbb{R}^N$, where x represents the 3D voxel coordinates, and N is the number of intensity values of multi-spectral MRI data for each voxel. Following this notation, when dealing with single-subject atlases, we can differentiate between the grey level volume, $\pi^I(x)$, defined as $\pi^I : x \in \mathbb{R}^3 \mapsto \pi^I(x) \in \mathbb{R}$, and the corresponding labelled volume, $\pi^L(x)$, defined as $\pi^L : x \in \mathbb{R}^3 \mapsto \pi^L(x) \in \mathcal{L}$, where $\mathcal{L} = \{1, \ldots, C\}$ and C is the number of labels. If probabilistic atlases are available, for each class c the probabilistic volume $\pi_c^P(x)$ is defined as $\pi_c^P : x \in \mathbb{R}^3 \mapsto \pi_c^P(x) \in \mathbb{R}$ where $c \in \{1, \ldots, C\}$.

By definition, volumes $\pi^I(x)$, $\pi^L(x)$ and $\pi_c^P(x)$ are on the same spatial coordinates, which we refer to as the *atlas space* $\mathcal{X}_\pi$. On the other hand, the input image usually lies in a different space, which we refer to as the *image space* $\mathcal{X}_I$. Therefore, in order to use the atlas information, a transformation $\tau : x_\pi \in \mathcal{X}_\pi \mapsto x_I \in \mathcal{X}_I$ must be found in the space of all possible transformations $\mathcal{T}$. The process of finding this transformation is commonly known as image registration and is defined in Eq. (1) as an optimisation problem, where $\hat{\tau}$ is the estimated transformation and $\delta()$ is a similarity metric used to compare the input image and the transformed intensity image volume of the atlas.

$$\hat{\tau} = \underset{\tau \in \mathcal{T}}{arg\max} \delta(I(x), \pi^I(\tau(x))). \quad (1)$$

Finally, we can define the final segmentation, $S(x)$, as $S : x \in \mathbb{R}^3 \mapsto S(x) \in \mathcal{L}$.

3.1. *Label propagation*

Once the registration problem is solved, the easiest and fastest way to assign a label to each input image voxel is to propagate the atlas labels to image space, $\mathcal{X}_I$ [20,42–52]. This segmentation procedure is defined as:

$$S(x) = \pi^L(\hat{\tau}(x)). \quad (2)$$

With this strategy, the segmentation process relies on a registration process that aims to estimate the anatomical differences between the atlas and the input image volumes. Registration errors exist in all real-world applications but errors are larger if differences between two images are large. We assume that the atlas is *close* to the subject's anatomy. Otherwise, in cases where large anatomical differences exist, large registration errors may cause important segmentation errors.

Global rigid and affine transformations are usually enough when dealing with intra-subject medical applications, such

as longitudinal studies of illness progression or multi-modal registration for radiotherapy planning. However, when dealing with inter-subject applications such as atlas matching, the anatomical variation between different subjects can only be captured using non-rigid algorithms.

Volume partitioning can be performed to account for these local deformations. In general, either the moving image (usually the atlas) or the target image or both image volumes are decomposed on smaller sub-volumes and these sub-volumes are then registered in a hierarchical manner using rigid and affine transformations [53–55].

Other partitioning approaches define a uniform grid, usually called the free-form deformation grid, and then apply a non-linear transform to each of the grid vertices. Depending on accuracy and time efficiency requirements, grid vertices can be defined as the voxels for the whole volume. Common non-linear transforms based on mathematic transformations are, for instance, cosine based functions [56], B-spline curves [8,57] or level set partial differential equations [58]. Other functions used to define a displacement field are based on the thermodynamics concept of demons [59,60], optical flow models [61,62] or elasticity properties [20,42].

3.2. Multi-atlas label propagation

Label propagation has been extended to multiple atlases to better deal with the registration errors obtained when using a single atlas and also to better account for anatomical variability. With an atlas database, those voxels with low agreement between different label propagations can be discarded in order to minimise outliers. Due to its strengths over simple label propagation, this technique presents an improvement in accuracy when dealing with the segmentation of objects with well-defined shape that may present slight deformations between images.

There are two important considerations to take into account when dealing with a set of atlases. The first is related to the number of atlases to be used to segment a new patient and how to select them. We refer to this issue as the selection criteria problem. Different studies [63–66] conclude that using more than one topological atlas improves accuracy, but that it is not necessary to use all the cases in a database.

Two principal methods exist for choosing the best matching cases: either using meta-information (which may not always be available), or using similarity metrics to compare the images. In order to use this second method, the new image must be aligned to all the manually segmented cases. One possible technique is to warp all atlases into a common space, and the subject to be segmented will then be matched in this space. This considerably reduces the number of registrations. However, with this strategy, there exists a strong dependency on the initially selected reference space. Therefore, new group-wise registration techniques [34–41] may prove a better way of solving this issue. These techniques try to register all the subjects together constructing an average reference template at each step. It is also advisable to use a combination of similarity metrics to avoid bias from using the same metric as in the registration step.

The question of how atlases should be combined remains. Voting rules are commonly applied [63–68]:

$$S(x) = \underset{c}{arg\max} \sum_{i=1}^{P} w_i(x) \cdot f(\pi_i^L(\hat{\tau}_i(x)), c), \tag{3}$$

where c represents a class, P is the number of atlases, w_i is a weight function that may vary for each atlas voxel and f is defined as:

$$f(\pi_i^L(\hat{\tau}_i(x)), c) = \begin{cases} 1 & : \pi_i^L(\hat{\tau}_i(x)) = c, \\ 0 & : \pi_i^L(\hat{\tau}_i(x)) \neq c. \end{cases} \tag{4}$$

This step can be seen as a specific case of classifier fusion. Within this voting procedure, the function $w_i(x)$ can either be defined as a constant value for all atlases to use a majority voting strategy [69,70] ($w_i(x) = 1/p$), a different constant value for each atlas to use globally weighted voting [71] ($w_i(x) = K_i$) or a function for each voxel to use locally weighted voting [68,72] ($w_i(x) = f_i(x)$). Recently, a generative probabilistic model for this fusion step was presented by Sabuncu et al. [73].

Other combination strategies based on the Expectation Maximisation (EM) algorithm have also been presented [74,75]. However, these methods usually obtain a lower accuracy when compared to local weighting methods [68]. Intuitively, these techniques weight each atlas according to estimated agreement or similarity with respect to the other atlases. However, in the case where the atlases with the highest agreement are not the best match for the subject being segmented, such a weighting procedure may bias the segmentation.

3.3. Probabilistic atlas-based segmentation

When probabilistic atlases are used, voxel probabilities can be integrated as part of a statistical Bayesian framework [55,76–83] as defined by:

$$S(x) = \underset{c}{arg\max} p(I(x)|c) \cdot p(c), \tag{5}$$

where $p(I(x)\,|\,c)$ represents the conditional probability of the intensities, and $p(c)$ are the class priors. Probabilistic atlases can also be used within variational frameworks [30,31,84–86]:

$$S(x) = \underset{c}{arg\min}(E_d + \lambda \cdot E_s), \tag{6}$$

where E_d is the data energy term, E_s is the smoothness energy term, and λ is a user-defined parameter.

Either parametric (for instance using Gaussian mixture models) or non-parametric approaches (for instance using Parzen windows) can be used to estimate $p(I(x)\,|\,c)$ and E_d. Initial estimates of such models often use propagation of the atlas probabilities [79,81,82,84]. Class priors ($p(c)$) and smoothness term (E_s) may also be encoded using atlas probabilities [83], sometimes in combination with other spatial priors [30,31,55,76–78,80,85,86] often modelled by Markov Random Models.

Table 1 – Advantages and drawbacks of the different reviewed atlas-based segmentation strategies.

	Description	Strengths	Challenges	Application
Label propagation (LP)	Atlas labels are directly applied in image space	Intuitive Straight-forward A single registration	No anatomical variability Atlas dependant Registration dependant	ROI definition or contour initialisation
Multi-atlas propagation (MA)	Multiple labels are combined in image space	Anatomical variability Outlier minimisation	Atlas selection and combination Multiple registrations	Segmentation of structures with a well-defined shape
Probabilistic atlas segmentation (PA)	Atlas values are used in a probabilistic framework	Anatomical variability A single registration Multiple input features	Atlas weighting Complex model estimation	Segmentation of new classes or classes with high anatomical variability

Some other methods [52,87–90] directly combine atlas probabilities with other image features such as voxel intensities or spatial coordinates (x) to train a classifier. These classifiers allow several features to be combined without the need to estimate a probability distribution in a high dimensional space.

The above-mentioned strategies use all the atlas probability values after registering the atlas with the patient. In order to reduce the effect of registration errors, some approaches select only a subset of voxel samples with high probability per class. These atlas samples can then be used to train a classifier [91–94], to estimate class distributions [95,96], or as initialisation points for a contour based segmentation [97].

3.4. *Summary*

In this section, we have presented three strategies for dealing with the information provided by an atlas (see Table 1 for a summary of the main advantages and drawbacks for each strategy). The most straightforward technique is to assign atlas labels after registration of the intensity atlas volume with the subject we wish to segment. This label propagation technique is highly dependent on both the atlas image and the registration procedure, and it may not be desirable when dealing with subjects from very different populations. Nevertheless, label propagation is widely used as a segmentation method to define a region of interest (ROI) for further segmentation [51,87,94] or to initialise an active contour strategy [49,98].

Furthermore, several topological atlases can be taken into account to improve the capture of anatomical variability between different scans. This multi-atlas propagation is in fact an extension of label propagation. Therefore, these techniques are desirable when segmenting objects with a well-defined shape where there is low anatomical variability between different images.

Finally, when using probabilities (either from a probabilistic atlas or a combination of topological atlases), a probabilistic model of the input images can be estimated. This probabilistic model, which may be unknown, can be estimated by different methods (i.e. parametric, non-parametric, or trained classifiers) that apply outlier rules to segment the images into new classes not present in the atlas. Moreover, these models may also be learned from a subset of image voxels to reduce the effect of registration errors.

4. Segmentation methods and clinical targets

Table 2 offers a compact overview of methods to segment the brain using atlas information. We have grouped the segmentation algorithms into four categories according to their medical target: (1) brain structures with well-defined shapes (such as the whole brain or the hippocampus), (2) brain tissues in healthy subjects (namely GM, WM and CSF), (3) brain tissues in challenging populations such as fetuses, neonates, and elderly subjects, and (4) damaged brains with either focal lesions (e.g. white matter lesions) or space-occupying lesions (e.g. tumours). Fig. 2 depicts the relation of these different categories with the types of atlases used. Table 2 also specifies the type of atlas used, the registration technique applied, and the corresponding atlas-based segmentation strategy.

In this section, we briefly describe these methods followed by a qualitative and quantitative evaluation of the results reported in the literature. We select the Dice similarity coefficient (DSC) as a measure for comparison since it is the most commonly used in the studies analysed (see Appendix A). Moreover, in Section 4.5, a summary of toolboxes freely available on the internet will be presented.

4.1. *The brain and its internal structures*

The brain itself may be the first structure to be targeted. The procedure of removing non-brain tissue is a well-known pre-processing step in brain imaging. Several reviews and comparisons have been presented recently [99–102], concluding that, among all brain segmentation methods, atlas-based segmentation (mainly by label propagation of probabilistic atlases) is applied as an initial step, although further processing is needed to obtain a good brain segmentation [103,104].

In this section, we focus on the segmentation of the internal structures of the brain such as the amygdala (AMY), accumbens (ACC), caudate (CAU), hippocampus (HIP), pallidum (PAL), putamen (PUT) or the thalamus (THA) (as shown in Fig. 3). Note that these structures present well-defined shapes that show some anatomical variability between subjects.

Table 2 – Classification of automated atlas-based segmentation methods. Rows are the segmentation targets, while columns refer to: the type of atlas, the number of volumes used to build the atlas, the registration method, and the atlas strategy (label propagation (LP), multi-atlas propagation (MA), and probabilistic atlas segmentation (PA)).

	Article	Atlas type		Registration transforms		Strategy
		Statistical	Topological	Global transforms	Local transforms	
Internal structures	Bajcsy [20]	No	1 manual	Affine	Elastic	LP
	Gee [42]	No	1 manual	Affine	Elastic	LP
	Miller [43]	No	1 manual	Affine	Mechanoelastic	LP
	Collins [44]	No	1 manual	Affine	Deformation vectors	LP
	Christensen [45]	No	1 manual	Affine	Fluid mechanics	LP
	Davatzikos [47]	No	1 manual	Affine	Elastic	LP
	Iosifescu [46]	No	1 manual	Affine	Elastic	LP
	Dawant [48]	No	1 manual	Affine	Demons	LP
	Baillard [49]	No	1 manual	No	Optical flow	LP
	Fischl [78]	12 manual	No	Affine	No	PA
	Klein [50]	No	1 manual	Affine	Mindboggle	LP
	Klein [63]	No	19 manual	Affine	Mindboggle	MA
	Heckemann [67]	No	29 manual	Affine	B-splines	MA
	Pohl [108]	80 manual	No	Affine	Hierarchical	PA
	Han [55]	80 manual	No	Affine	Hierarchical	PA
	Bazin [31]	18 manual	1 manual	Rigid	No	PA
	van der Lijn [80]	19 manual	No	Affine	B-splines	PA
	Aljabar [65]	No	275 manual	Affine	B-splines	MA
	Artaechevarria [68]	No	18 manual	Affine	B-splines	MA
	Ciofolo [52]	No	1 manual	Rigid	Hierarchical	LP
	Lötjönen [66]	No	17 manual	Affine	Hierarchical	MA
Healthy tissue	Van Leemput [76]	ICBM	No	Affine	No	PA
	Marroquin [84]	ICBM	No	Affine	Level set	PA
	Cocosco [91]	53 manual	No	Affine	No	PA
	Grau [97]	29 manual	No	No	Demons	PA
	Ashburner [114]	ICBM	No	Affine	Cosine	PA
	Awate [79]	ICBM	No	Affine	No	PA
	Vrooman [92]	22 manual	No	Affine	B-Splines	PA
	Bricq [82]	ICBM	No	Affine	B-splines	PA
Fetus, neonates, elderly	Mortamet [125]	ICBM	No	Affine	No	PA
	Prastawa [118]	3 manual	No	Affine	No	PA
	Weisenfeld [116]	13 manual	No	Affine	No	PA
	Xue [119]	No	3 manual	Affine	No	LP
	Murgasova [120]	1 manual (37)	No	Affine	B-Splines	LP,PA
	Smith [126]	141 manual	No	Affine	Cosine	PA
	Habas [122,124]	14 manual	No	Affine	Elastic	PA
	Weisenfeld [117]	15 manual	No	Affine	No	PA
Damaged brains						
Focal lesions	Kamber [87]	12 manual	No	Rigid	No	LP, PA
	Van Leemput [77]	ICBM	No	Affine	No	PA
	Zijdenbos [88]	53 manual	No	Rigid	No	PA
	Wu [51]	Yes	No	Affine	B-splines	LP
	Bricq [81]	31 manual	No	Affine	B-splines	PA
	Kroon [89]	ICBM	No	Affine	B-splines	PA
	Prastawa [96]	ICBM	No	Affine	No	PA
	Shiee [85,86]	18 manual	1 manual	Rigid	No	PA
	Souplet [83]	ICBM	No	Affine	No	PA
	Akselrod-Ballin [90]	ICBM	No	Affine	Cosine	PA
	de Boer [93]	No	12 manual	Affine	B-splines	PA
	Tomas [94]	15 manual	15 manual	No	B-splines	LP, PA
	Shiee [30]	18 manual	1 manual	Rigid	No	PA
Space-occupying lesions	Kyriakou [142]	No	1 manual	Affine	Elastic	LP
	Dawant [143]	No	1 manual	Affine	Demons	LP
	Warfield [148]	No	1 manual	No	Elastic	LP
	Moon [154]	ICBM	No	Affine	No	PA
	Shen [149]	1 manual	1 manual	Affine	Hierarchical	LP
	Bach Cuadra [145]	No	SPL	Affine	Demons	LP
	Duay [151]	No	1 manual	No	Elastic	LP

– Table 2 (*Continued*)

Article	Atlas type		Registration transforms		Strategy
	Statistical	Topological	Global transforms	Local transforms	
Liu [153]	No	1 manual	Affine	Hierarchical	LP
Prastawa [95]	ICBM	No	Affine	No	PA
Stefanescu [152]	No	1 manual	Rigid	Grid-based	LP
Pollo [146]	No	SPL	Affine	B-Demons	LP
Nowinski [147]	No	1 manual	No	Non-linear	LP
Bach Cuadra [140]	No	SPL	Affine	Optical flow	LP
Zacharaki [150,141]	No	1 manual	Affine	Elastic	LP

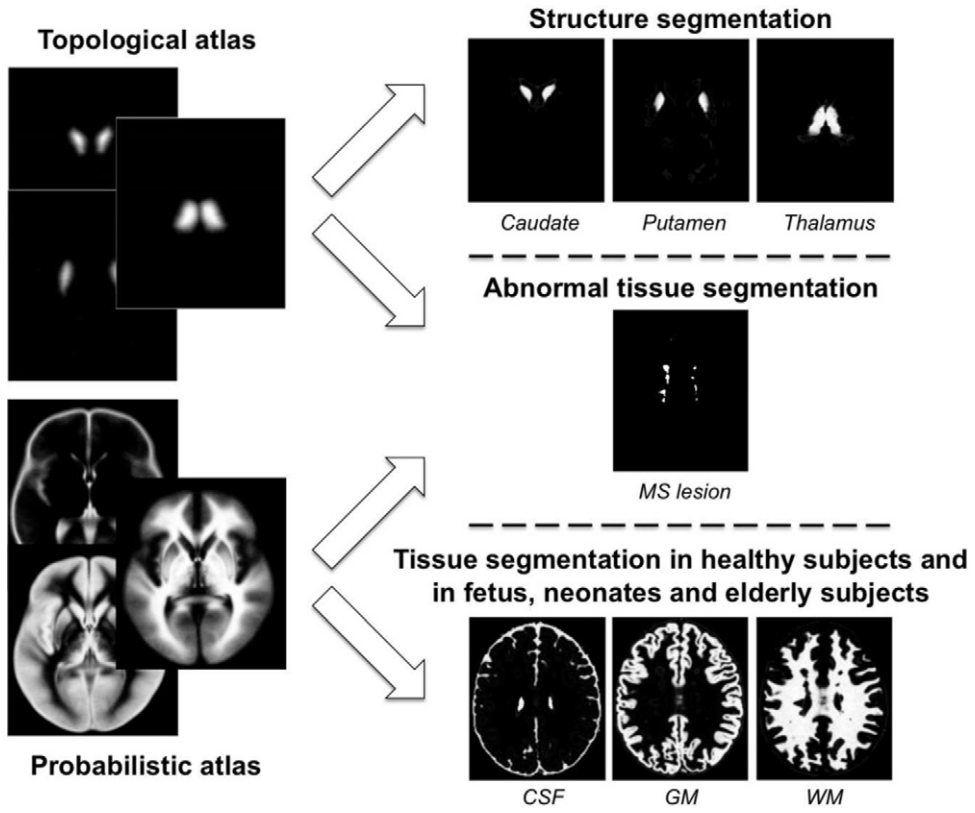

Fig. 2 – Diagram of how atlases are used to segment structures, healthy tissue (in both healthy and challenging population) and abnormal tissue and lesions. The MR brain data sets and their manual segmentations were provided by the Center for Morphometric Analysis at Massachusetts General Hospital and are available at http://www.cma.mgh.harvard.edu/ibsr/.

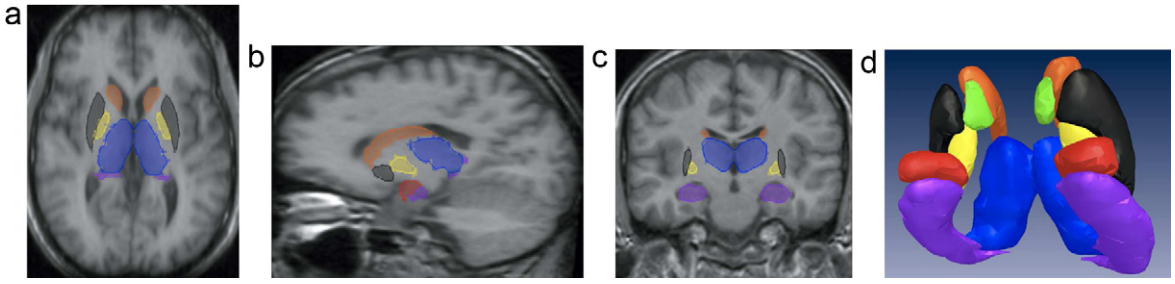

Fig. 3 – Internal structures of the brain. (a) Axial plane, (b) sagittal plane, (c) coronal plane, and (d) 3D representation of the following structures: thalamus (blue), putamen (black), pallidum (yellow), hippocampus (purple), caudate (orange), amygdala (red) and accumbens (green). (For interpretation of the references to color in this figure legend, the reader is referred to the web version of the article.)

Due to the lack of clearly defined edges between some brain structures and substructures, approaches based solely on voxel intensities are expected to produce poor results [78]. Therefore, a priori spatial information for anatomical structures is required. Several studies have adopted label propagation strategies, focusing their contribution on developing new registration techniques based on, for instance, elasticity [20,42,43,46,47], deformation vectors [44], fluid mechanics [45], thermodynamics [48], optical flow [49] or hierarchical methods [50]. Propagated labels can later be extended to define a fuzzy label map (with higher values for voxels inside the label masks and lower values for voxels outside the masks) guiding a fuzzy controller. For instance, Ciofolo and Barillot [52] designed a fuzzy controller to guide a competitive level set approach initialised by cubes inside the brain scan.

As mentioned in Section 3, multi-atlas approaches have become a recent area of research on automated atlas-based segmentation to provide improved capture of anatomical variability. Heckemann et al. [67] proposed the combination of 29 topological atlases after registration via a vote rule decision fusion approach. This technique treats each propagation as a separate classifier and then applies the label with the maximum number of occurrences to each voxel. A similar study by Klein et al. [63] assigned a structure label to each voxel by applying the findings of their previous study [50] on 19 atlases.

When using a large database with previously segmented cases some of the segmentations can deviate greatly from the new subject and therefore bias the result and decrease segmentation accuracy. To resolve this issue, Aljabar et al. [65] presented a new approach based on selecting a subset of volumes instead of using all 275 cases (the total number of volumes in the database). The selection was based on taking both volume similarity and meta-information into account. Moreover, as pointed out by Artaechevarria et al. [68], even if the best atlases are chosen, their variability can affect the final result depending on the fusion technique applied. In this last study, the authors proposed different weighting methods: either globally, using similarity measures for the whole volume, or locally, using a small neighbourhood area. In their study, local methods were found to improve the final segmentation when compared to global methods. The same conclusion was obtained by Lötjönen et al. [66], who reviewed selection and combination algorithms as well as non-rigid registration. Furthermore, they noticed that although atlas selection methods provided better segmentation results than random selection, there was still a clear difference with respect to the results obtained when knowing the optimal set of atlases.

While these studies create a statistical atlas and keep the labels with the highest probability per voxel, there are others that use atlas probabilities on a complex statistical framework (mainly based on Bayes theorem). For instance, van der Lijn et al. [80] created a probabilistic atlas by averaging different topological atlases and then incorporated those probabilities as an energy term in a graph-cuts segmentation approach.

Fischl et al. [78] proposed segmenting brain structures using the Iterated Conditional Modes (ICM) algorithm [105] after defining the transformation between a probabilistic atlas and the subject. This optimisation algorithm starts with initial estimates for the parameters, called conditional modes, and proceeds to update the segmentation sequentially until the optimum is found. In this case, the volume is defined as a Markov Random Field (MRF) to explicitly include spatial information. The ICM is initialised with the maximum a posteriori (MAP) estimate of the segmentation. In a subsequent work, Han and Fischl [55] proposed applying a pre-processing step to this framework, consisting in atlas intensity normalisation for enhancing the performance on different scanning platforms.

In a similar way, segmentation and registration can be combined in a probabilistic framework via an EM algorithm [106] or the Fuzzy C-Means (FCM) [107] algorithm. The EM algorithm computes the probability of each entry of the data set belonging to a certain distribution. It then estimates the hidden parameters of this distribution which maximise the previous expectation in an iterative manner until convergence is reached. Even though great convergence properties are found, this algorithm can lead to non-desired local minima, especially when only relying on the data itself. Therefore, proper initialisation and spatial information are introduced into the framework using atlas-based approaches. For instance, Pohl et al. [108] proposed using the EM algorithm to find the optimum parameters for registration while labelling each voxel to a brain structure. On the other hand, FCM inherently treats each class as a Gaussian with the same variance, since it only takes class centroid and membership values for each voxel into account. Note that no spatial information is encoded in the original algorithm. However, Bazin and Pham [31] proposed modifying the objective function to include spatial constraints as well as probabilities from a statistical atlas. Segmentation masks were then constrained by a topological atlas to ensure that topology was preserved. Finally, growing and thinning techniques were used to refine the final delineations of the brain structures.

Regarding the experimental evaluation of these works, the Dice Similarity scores for the central nuclei (amygdala, accumbens, caudate, hippocampus, pallidum, putamen, and thalamus) are summarised in Table 3. This table includes information about the data sets used for validation. Even if some of the approaches [31,52,66,68] use the same data set (IBSR), a quantitative comparison of all methods is difficult due to the variability of the testing data. Furthermore, the number of cases used for testing varies, ranging from 10 to 30 volumes, with the exception of Aljabar et al. [65], who used a larger database of 275 subjects to show the influence of atlas selection.

We would like to point out that the results obtained by Klein et al. [50,63] are not included since they provide similarity values for the whole brain instead of structure-based values. However, in their last study, the authors provided a comparison of the similarity values when increasing the number of atlases, showing also an increase in the Dice coefficient. This behaviour can also be observed in Table 3, where the best Dice values for each structure are obtained from multi-atlas approaches [65–67], closely followed by statistical frameworks [55,78,108]. Notice that Aljabar et al. [65] obtained the best results on some structures (the thalamus, the hippocampus, and the accumbens) by applying selection strategies in their multi-atlas approach. Furthermore, among the approaches using IBSR data, the method of Lötjönen et al. [66] outper-

Table 3 – Summary of brain structure segmentation results using the DSC metric. Additional information on the number of volumes (*v*) and the MRI system is also given. Acronyms in alphabetical order: Amygdala (AMY), Accumbens (ACC), Caudate (CAU), Hippocampus (HIP), Pallidum (PAL), Putamen (PUT), and Thalamus (THA).

Article	Real data							
	CAU	THA	PUT	PAL	HIP	AMY	ACC	Test data (MRI system)
Dawant [48]	0.86	–	–	–	–	–	–	8*v* (Siemens 1.5T)
Fischl [78]	0.88	0.79	0.71	0.71	0.81	0.79	–	14*v* (GE 1.5T) + 13*v* (Siemens 1.5T)
Klein [a] [50]	–	–	–	–	–	–	–	10*v* (Siemens 3T)
Klein [a] [63]	–	–	–	–	–	–	–	10*v* (Siemens 3T) + 10*v* (GE 1.5T)
Heckemann [67]	0.90	0.90	0.90	0.80	0.81	0.80	0.70	30*v* (GE)
Pohl [108]	–	0.894	–	–	–	–	–	22*v* (GE 1.5T)
Han [55]	0.84	0.88	0.85	0.76	0.83	0.75	–	14*v* (GE 1.5T) + 13*v* (Siemens 1.5T)
van der Lijn [80]	–	–	–	–	0.858	–	–	20*v* (Siemens 1.5T)
Bazin [31]	0.781	0.773	0.817	–	–	–	–	18*v* (IBSR)
Aljabar [65]	0.881	0.908	0.898	0.818	0.834	0.777	0.758	275*v* [b]
Artaechevarria [68]	0.83	0.88	0.87	0.81	0.75	0.72	0.68	18*v* (IBSR)
Ciofolo [52]	0.60	0.77	0.66	0.56	–	–	–	18*v* (IBSR)
Lötjönen [66]	0.866	0.899	0.905	0.844	0.819	0.767	–	18*v* (IBSR)

[a] Results by Klein et al. [50,63] are reported for the brain as a whole rather than providing values for each structure.
[b] Aljabar et al. [65] do not specify the MRI system used.

formed the others for all structures. Note that this method is also based on a multi-atlas strategy.

Only few studies focus on evaluating how algorithms are affected by image variability within different scanning devices. For instance, Klein et al. [50,63] and Han and Fischl [55,78] validated their methods with MRI data acquired from different machines. This later study also demonstrated the importance of normalising the atlas and the subject intensities when using different scanning machines, obtaining higher DSC values after atlas normalisation when using data sets from two different MRI scanners. Almost all of the studies in Table 3 segment images from 1.5T devices. Only Klein et al. [50,63] applied their method to MRI images acquired at higher magnetic fields (3T). The recent multi-site and multi-scanner database maintained by the Alzheimer's Disease Neuroimaging Initiative (ADNI) [109] will allow researchers to test the robustness of developed algorithms on different scanning devices.

Segmentations for central nuclei structures have a DSC of between 0.70 and 0.90, showing good agreement between manual and automatic segmentation. The best segmentation results are obtained for the caudate, the thalamus, and the putamen structures, with values of 0.90, while the segmentations of the amygdala, the hippocampus, and the accumbens achieve values near 0.80 when using multi-atlas strategies.

4.2. *Brain tissue segmentation in healthy subjects*

MRI has become a standard modality for brain tissue segmentation due to its high effectiveness in contrasting between tissue types. However, some image artefacts like the partial volume effect, image noise and intensity non-uniformities (also known as bias field [110]) can considerably increase the difficulty of segmentation work. In addition to these artefacts, the large differences that may exist between sulci and gyri patterns for various subjects are the main issues when dealing with brain tissue segmentation.

Numerous approaches have been proposed for MR brain tissue segmentation [111–113] and only some use atlas priors. Atlas-based approaches for brain tissue segmentation are mostly within a statistical framework and make use of probabilistic atlas priors (see Section 3.3).

Van Leemput et al. [76] proposed accounting for neighbouring relationships between voxels through an MRF model. Distribution parameters were then estimated using the EM algorithm using bias field estimation to aid the segmentation task. Due to the need for initialisation, the authors decided to use atlas probabilities as a prior classification and to constrain the classification process at each iteration by multiplying the E-step probability by the one given by each atlas voxel. In a similar way, Bricq et al. [82] proposed including Markovian properties to account for voxel relationships by means of hidden Markov chains. After applying this theory to MRI, model parameters were also estimated with EM using atlas probabilities during initialisation and each subsequent iteration step. In order to increase the robustness, Marroquin et al. [84] proposed a novel variant of the EM algorithm which also relies on atlas information for initialisation. This algorithm substitutes the expectation step by using the MAP estimator to compute the MRF parameters followed by the maximiser of posterior marginal estimate instead of the maximisation step. Therefore, using the atlas values for initialisation, this algorithm iterates until convergence is achieved.

While most segmentation approaches using Markov theory rely on a parametric estimation, non-parametric methods are quite powerful themselves, as pointed out by Awate et al. [79]. In their study, the Parzen-window technique is used to estimate a Markov probability density function (PDF) without imposing strong parametric models on the data. This data-driven technique, which is also initialised using atlas probabilities, provides the ability to model and learn arbitrary PDFs. However, corrupted volumes may bias this estimation and cause misclassification errors.

All the above methods rely on an initial registration step and then apply a segmentation framework. However, both steps are closely related, since atlas registration can benefit from an initial segmentation, while brain tissue segmentation requires prior information such as atlas probabilities,

which are obtained from the atlas registration process. Hence, by combining both steps, Ashburner and Friston [114] proposed a novel method for segmenting brain tissues while correcting the bias field and refining atlas registration. In their approach, the ICM algorithm is used to estimate the final segmentation, while Gaussian Mixture Model parameters are estimated via EM using atlas probabilities and volume intensity. A Levenberg–Marquardt algorithm is then applied to correct the bias field and refine atlas alignment.

Probabilistic atlases can also be translated to topological ones. By applying a threshold to the probabilities, topological masks may be obtained for each tissue. Once registered to the subject volume, these masks can be applied in order to select a set of representative tissue samples from the subject. These are the samples that are then used to train a classifier. This is the main idea of the approach by Cocosco et al. [91] and Vrooman et al. [92], who extracted tissue samples using an atlas and then used the minimum spanning tree algorithm to reduce outliers. These samples were used to train a k-Nearest Neighbour (kNN) classifier. This algorithm uses the distance in feature space between the current voxel and each training sample to assign the label with most votes from among its k closest neighbours. Although this algorithm proposes a simple implementation, its major drawback is its high computational cost. Similarly, Grau et al. [97] applied the watershed transform to segment tissues. The simple and intuitive foundation of this algorithm consists in simulating the flooding of a region while considering image intensities as heights. However, one of the major drawbacks associated with this approach is that the obtained results may be over-segmented. The authors proposed setting some initial markers, corresponding to each tissue class, to overcome this issue. Skeletons are calculated by thresholding a statistical atlas and then removing outliers; the resulting skeletons are considered as the initial markers.

The lack of a gold standard for brain tissue classes in real images makes the quantitative evaluation of segmentation algorithms difficult. The BrainWeb phantom [23] provides a standard platform for comparing healthy brain approaches, but results on synthetic phantoms cannot be extrapolated to real conditions. Table 4 summarises the results for WM and GM on both synthetic and real data,[1] including also information on data acquisition. The number of volumes used to test the methods ranges between 10 and 40, which does not significantly differ from the reviewed segmentation methods for brain structures.

Contrary to the methods presented in Section 4.1 for deep brain structure segmentation, no tissue segmentation methods rely on label or multi-atlas propagation. Moreover, most brain tissue segmentation uses statistical atlases instead of topological ones. Tissue segmentation strategies are often based on probabilistic atlas segmentation. Furthermore, parametric estimation algorithms are most widely used, with DSC values over 0.90 on the BrainWeb phantom. For instance, values of 0.975 for GM and 0.980 for WM (both close to perfect agreement) are reported by Bricq et al. [82], who used the EM algorithm with atlas probabilities for initialisation and then include prior probabilities at each step.

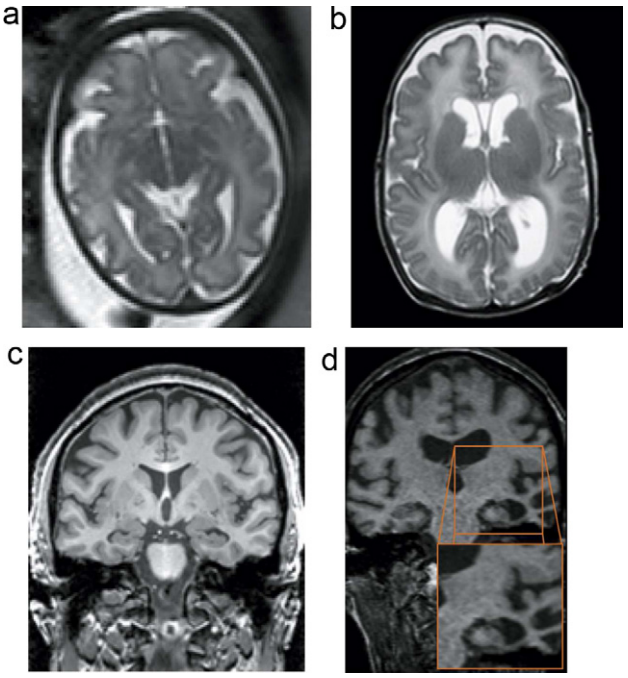

Fig. 4 – (a) Fetus at 31 weeks of gestational age, (b) premature newborn, (c) 61 year-old woman and (d) 66 year-old woman with dementia.

Even though significant agreement is found for synthetic data, DSC values decrease when these methods are applied to real cases. Awate et al. [79], who obtained worse results than Bricq et al. [82] when evaluating the BrainWeb phantom, obtained better results when testing with real data. These prove the need to use real data sets in conjunction with synthetic phantoms to evaluate and compare segmentation methods.

4.3. *Brain tissue segmentation in fetus, neonates, and elderly subjects*

There are specific populations such as fetuses and newborns that are particularly challenging for atlas-based segmentation methods. Automated segmentation of these populations is a key tool for brain development studies. Their specific characteristics (such as spatial and temporal variations of the image contrast due to myelination and folding of the growing brain, and low signal to contrast ratio and high partial volume effects due to fast acquisition sequences to avoid motion) represent new challenges for brain tissue segmentation when compared to adult brain segmentation. Consequently, on the one hand, anatomical priors are needed to reduce the complexity of segmenting fetus and neonate brains, while on the other hand constructing these atlases is difficult due to the constantly evolving anatomy. Fig. 4a and b shows intra-utero fetal and newborn brains, respectively.

Pioneer studies on these populations were carried out on newborns and pre-term infants. Some groups proposed supervised classification methods [115–118] using both MR

[1] CSF is not included since some methods do not include it in their segmentation.

Table 4 – Summary of healthy tissue segmentation results with DSC metric. Results are given for both real and BrainWeb images, where available. Additional information is also given on number of volumes (v) and MRI system.

Article	BrainWeb		Real data		
	GM	WM	GM	WM	Test data (Scanner)
Van Leemput [76]	0.93	0.92	0.836	0.821	9v (GE 1.5T)
Marroquin [84]	0.891	0.892	0.797	0.812	20v[b]
Cocosco [a] [91]	–	–	–	–	43v[b]
Grau [97]	0.890	0.946	–	–	–
Ashburner [114]	0.932	0.961	–	–	–
Awate [79]	0.92	0.96	0.807	0.887	18v[b]
Cocosco [92]	–	–	0.915	0.937	12v[b]
Bricq [82]	0.975	0.980	0.799	0.865	18v[b]

[a] Results by Cocosco et al. [91] are reported using the kappa similarity measure.
[b] Means that the MRI system used is not specified.

signal (multi-spectral contrast in some cases) and spatial priors. Probabilistic atlases are either used to train the classifier [117] or to be included as features for classification [118]. Bayesian frameworks (see Eq. (5)) for neonatal segmentation were suggested in [119]. Label propagation was used prior to the non-supervised statistical tissue segmentation to mask some structures. A label propagation approach [120] has also been presented to create a population-specific atlas for young children.

Very few studies exist related to the automated segmentation of fetal brain tissues [121–124]. Indeed, only one research group has recently proposed a spatio-temporal probabilistic atlas and an atlas-based segmentation of developing brain tissues in young fetuses [122,124].

Elderly subjects (see Fig. 4c) are another challenging population due to the loss of tissue volume related to ageing [125–127], also known as normal atrophy [128]. Still, the same registration methods are used as for young subjects. In this context, special attention needs to be paid to atlas selection and in cases where younger atlases are not representative of the elderly anatomy age and sex-specific atlases [129] can be used. It should be noted that the aging effect is also present in brains containing abnormal regions.

4.4. *Segmentation of tissues and lesions in pathological brains*

Abnormal atrophy (see Fig. 4d) is a common feature among neuro-degenerative brain disorders such as mild cognitive impairment, Alzheimer's disease, or schizophrenia. This pathological tissue loss[2] is not present on healthy atlases and is thus usually overlooked under the assumption that the registration step will capture it. As for healthy elderly subjects, the strategies presented in the previous sections are also used on these cases [67,130–134]. Disease-specific atlases could be used to improve segmentation results [32,33].

Damaged brains may contain more than subtle brain tissue loss, such as, for instance, focal tissue lesions or large space-occupying lesions. Obviously, atlases do not contain such damaged areas as they vary greatly in size, shape and location. Therefore, new strategies or extensions to existing methods are needed to deal with these pathological cases. Below, we distinguish between two kind of brain lesions. First, focal tissue lesions, which represent those produced by the loss and inflammation of tissue, as in strokes and multiple sclerosis. In these cases, registration error due to lesion areas not present in the atlas are neglected. Second, space-occupying lesions, like tumours, which induce a deformation on the patient's brain anatomy and where the deformation field caused by the lesion needs to be estimated.

4.4.1. *Focal tissue lesions*

Segmentation methods that deal with focal tissue lesions usually rely on the use of healthy brain atlases to segment brain tissues and consider lesions as *outliers*. Fig. 5 illustrates some examples of focal tissue lesions.

Shen et al. [135,136] proposed to automatically detect stroke lesions by comparing voxel-to-voxel the inconsistency between the result of applying an unsupervised tissue segmentation of the patient scans and the probability priors obtained within an atlas. Those regions where the inconsistency is large are assumed to be part of the lesion.

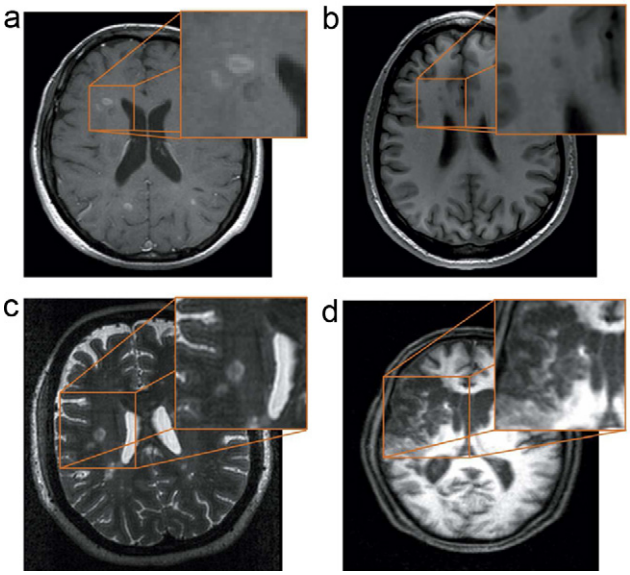

Fig. 5 – Focal tissue lesions. (a) Enhancing MS lesions, (b) black holes in MS, (c) hyperintense MS lesions and (d) medial cerebral artery ischaemia.

[2] Note that the tissue loss due to aging is present as well.

In most cases, following detection of the outliers a subsequent analysis is usually performed to ensure that outlier regions are actually lesions. These methods can be seen as an extension of healthy tissue and structure approaches that use a statistical frameworks, introducing a new class into the segmentation algorithm. For instance, Seghier et al. [137] extended the tissue segmentation approach of Ashburner and Friston [114] to detect stroke lesions. On the other hand, Van Leemput et al. [77] extended their previous work [76] to detect multiple sclerosis lesions by searching for outliers that follow a set of user-defined rules, i.e. lesions should appear as hyperintense on both PD-w and T2-w images. In a similar way, Bricq et al. [81] applied their hidden Markov chain approach [82] to detect multiple sclerosis lesions as outliers, while Shiee et al. [30,85,86] modified their fuzzy segmentation algorithm [31] to segment lesions inside WM tissue.

Similarly, Souplet et al. [83] extended a previous study by Dugas-Phocion et al. [138] based on segmenting tissues with an EM approach by including pure tissue and partial volume classes. Using pure tissue masks, normal appearing tissue parameters (mean and standard deviation) were estimated on the T2-FLAIR image to define a lesion threshold.

The unsupervised methods mentioned above can be biased by unhealthy tissues. Intuitively, supervised methods relying on tissue samples from lesion and non-lesion classes should perform better than unsupervised methods, since no intensity distribution models are assumed. For instance, Kamber et al. [87] compared three different classifiers. In their study, a probabilistic atlas was used to provide the classifiers with features as well as to constrain the search within the WM areas. Following the same idea, Wu et al. [51] implemented a kNN classifier trained on 20 voxels for each class. Following classification, a probabilistic atlas was used to relabel GM and multiple sclerosis lesions taking WM regions into account.

On the other hand, Zijdenbos et al. [88] used a probabilistic atlas to extract features for training an artificial neural network classifier. The input features included three MRI modalities and three spatial tissue priors from the atlas. Furthermore, healthy atlases could be extended, as proposed by Kroon et al. [89]. In this study, segmented lesions were manually warped to the ICBM atlas (from SPM) and this was used as a feature of a PCA-based classification framework which was trained with lesion and non-lesion samples. Developing a more general framework, Akselrod-Ballin et al. [90] proposed segmenting the volume in different regions using a graph-based algorithm. These regions were then characterised with a rich set of extracted features (comprising probabilities taken from an atlas) and classified using a decision forest along with the Fisher linear discriminant. This combination of segmentation and region classification helped to reduce misclassification at voxel level due to noisy data.

Atlases can also be used to sample healthy-looking tissue voxels. For instance, de Boer et al. [93] extended the healthy tissue classification from Cocosco et al. [91] to deal with white matter lesion segmentation. Similarly to Souplet et al. [83], after tissue segmentation a histogram of all GM voxels in T2-FLAIR is created and a threshold is defined to segment the lesions.

Atlases also provide a way to select abnormal tissue samples while estimating healthy ones. For example, Prastawa et al. [95,96] proposed using the Minimum Covariance Determinant to estimate tissue PDFs using healthy samples. Outliers to this estimation are then considered as abnormal tissue.

Finally, a combination of training sample points and WM area refinement for multiple sclerosis segmentation was presented by Tomas and Warfield [94]. This approach used a set of topological atlases to define healthy tissue samples, obtained using the STAPLE algorithm [74], and to create a probabilistic atlas from the average of these manual segmentations. Multiple sclerosis samples were then defined as intensity outliers by comparing the reference group and the subject volumes. Subsequently, a Bayes classifier was trained to select lesion and non-lesion voxels. Since some of these voxels were misclassified as false positives, this classification was refined using WM regions extracted from the probabilistic atlas.

Different lesion sizes and locations make the comparison of segmentation methods even more challenging than the evaluation for segmenting healthy brain tissue and structures. Furthermore, evaluation measures would differ for different lesion sizes and types (multiple sclerosis, strokes or tumours). Public data sets for lesions along with ground truth segmentations are rare. As far as we know, only the BrainWeb site [23] provides a public synthetic phantom to validate multiple sclerosis lesions, and data for only 20 subjects from the training set of the 2008 Multiple Sclerosis Challenge [139] are available.

Results with both synthetic and real data for white matter lesions are summarised in Table 5, including information on data acquisition. The number of tested subjects ranges between 10 and 30 for these studies, with the exception of de Boer et al. [93], who used 209 volumes to validate their method. Similarly to methods used for structure and healthy brain tissue segmentation, abnormal tissue segmentation approaches are validated using a small number of cases. Validation with larger data sets would be desirable in order to assess their usability in clinical practice.

As with approaches used for healthy tissue segmentation, brain tissues and lesions are mostly segmented using a probabilistic atlas segmentation framework. This is because most lesion segmentation methods are extensions of approaches used for healthy tissue segmentation. Note also that white matter regions are often used to confine lesions to a region of interest in order to reduce false positives.

Finally, we would like to briefly recall here the quantitative results published during the 2008 Multiple Sclerosis Challenge[3] [139]. A total of 53 volumes were separately acquired by the Children's Hospital Boston (CHB) and the University of North Carolina (UNC) for this competition: 20 volumes for training, 25 public volumes before the contest for validation and 8 volumes for on-site testing. Five of the nine methodologies presented during the challenge used an atlas-based strategy [81,83,86,89,96] with the best results of the competition obtained by Souplet et al. [83], using an EM algorithm initialised with atlas probabilities.

[3] All this information can be found at: http://grand-challenge2008.bigr.nl/ and the open journal www.midasjournal.org/browse/publication/638.

Table 5 – Evaluation of reviewed methods for abnormal tissue segmentation. DSC is presented for both real and BrainWeb simulated data, where available. Additional information is also given on number of volumes (*v*) and MRI acquisition devices. Studies presented in the MS Grand Challenge 2008 are not reported here since different evaluation measures were used and only off-site results are provided for all of them.

Article	BrainWeb	Real data	
	Abnormal	Abnormal	Test data (Scanner)
Kamber [a] [87]	–	–	12*v* (Philips 1.5T)
Van Leemput [77]	–	0.49	23*v* (Philips 1.5T)
Zijdenbos [88]	–	0.60	29*v*[b]
Prastawa [95]	–	0.854	3*v*[b]
Wu [51]	–	0.6	12*v* (Siemens 1.5T)
Shiee [85]	0.677	0.531	10*v* (Philips 3T)
Akselrod-Ballin [90]	–	0.53, 0.55	25*v*[b] + 16*v*[b]
de Boer [93]	–	0.72	209*v* (GE 1.5T)
Tomas [94]	–	–	9*v* (GE 3T)
Shiee [30]	0.789	0.633	10*v* (Philips 3T)

[a] Results by Kamber et al. [87] are reported using error measures.
[b] Means that the MRI system used is not specified.

4.4.2. *Space-occupying lesions*

Examples of space-occupying lesions are shown in Fig. 6. These lesions induce large deformations and lack clear anatomical detail due to infiltration and edema [12], making the registration of diseased brains with normal atlases difficult. When space-occupying lesions are present, registration methods aim to capture not only the anatomical variability but also the deformations induced by the tumour. Thus the assumption of small and smooth deformations is clearly violated [140,141].

The original works of applying atlas-based segmentation to the presence of tumours were by Kyriakou and Davatzikos [142] and Dawant et al. [143]. The aim of both approaches was to estimate how the presence of the lesion affected brain tissues and structures. The approach of Kyriakou and Davatzikos [142] modelled the soft tissue deformations induced by the tumour using a finite-element method, and subsequently, they registered the topological atlas with a transformed patient image from which the tumour was removed. As for Dawant et al. [143,144], the patient (including the tumour) was registered with a seeded version of the atlas that included a region with the same intensity properties as the tumour, which was manually segmented previously. Bach Cuadra et al. [145] and Pollo et al. [146] improved this approach by avoiding registration of the full volumes, assuming a radial tumour growth from a single voxel seed. A similar assumption was taken into account by Nowinski and Belov [147], who proposed a non-linear tumour deformation after registration of the patient volume and the atlas using Talairach registration. All these methods required a precise pre-segmentation of the tumour, usually performed using semi-automatic algorithms [148]. More sophisticated models of lesion growth are proposed by the authors of the HAMMER [149] and the ORBIT [150,141] frameworks.

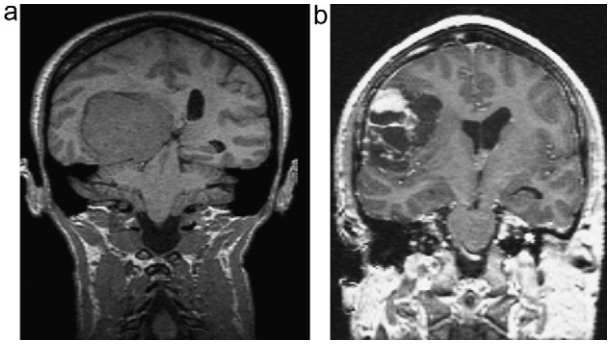

Fig. 6 – Space-occupying lesions: (a) meningioma and (b) astrocytoma.

Some other methods [151–153], instead of having a lesion growth model, apply different rigidity constraints to the tumour area. For instance, Duay et al. [151] locally adapt the elasticity of the transformation, hence allowing large deformations around the tumour. Pre-segmentation of the tumour was not necessary. Stefanescu et al. [152] introduce specific rigidity parameters for the tumour, and Liu et al. [153] assume local rigidity by means of a Markov Random field-maximum a posteriori approach. However, both approaches again require a priori segmentation of the lesion.

Moon et al. [154] extended Van Leemput et al.'s [76] tissue segmentation approach for detecting brain tumours. The authors used the same EM approach but extended the number of classes with a tumour class. The prior spatial probabilities of the tumour location were introduced into the algorithm by multiplying the atlas probabilities by the difference image of the pre and post-contrast images. Prastawa et al. [95], prior to detecting MS lesions as seen in Section 4.4.1, also proposed detecting tumours and edemas by using the Minimum Covariance Determinant to estimate tissue PDFs using healthy samples, and determining the diseased regions as the resulting outliers of the model.

Results for tumours [95] (DSC of 0.854 using only 3 cases) and general white matter lesions [93] (DSC of 0.72 using a large data set of 209 cases) show a good agreement in real data. Unfortunately, in the specific case of WM lesions corresponding to MS lesions, segmentation results show lower DSC values, like, for instance, the 0.633 obtained by Shiee et al. [30] using a statistical framework based on the fuzzy clustering algorithm. This indicates that there is a need for further development of MS lesion segmentation.

4.5. *Publicly available toolboxes*

Some of the methods reviewed in this paper are publicly available as toolboxes, open source code or closed applications. For instance, the structure segmentation methods proposed by Collins et al. [22] and Fischl et al. [78] are publicly available as part of the ANIMAL (www.bic.mni.mcgill.ca/ServicesSoftwareAdvancedImageProcessingTools/RegistrationTools) and FreeSurfer (http://surfer.nmr.mgh.harvard.edu/) applications, respectively. Similarly, FSL presents a set of brain MRI tools called FIRST, which also include an atlas-based tool to segment structures (http://www.fmrib.ox.ac.uk/fsl/). Furthermore, Ashburner et al.'s [114] tissue segmentation method is implemented as part of the MATLAB toolbox SPM (www.fil.ion.ucl.ac.uk/spm/). Another tissue segmentation method based on the SPM code was implemented and made available by Van Leemput et al. [76] under the name Expectation Maximisation Segmentation (EMS) (www.medicalimagecomputing.com/downloads/ems.php). Finally, Zijdenbos et al. [88] and Souplet et al. [83] also made their methods available as part of the INSECT (www.bic.mni.mcgill.ca/ServicesSoftwareAdvancedImageProcessingTools/HomePage) and SepINRIA (www-sop.inria.fr/asclepios/software/SepINRIA/) applications, respectively. Note that these public toolboxes provide also a public atlas (the one used in their algorithms), for instance, the Desikan's atlas [155] within the Freesurfer package or probabilistic atlases within SPM. We would also like to point out the importance of other development platforms such as the Insight Toolkit (ITK, www.itk.org/). A wide range of registration and segmentation techniques are distributed within this C++ library for image processing. Moreover, a large number of developers have used this library as the core to implement medical image processing tools or to develop their own toolboxes, such as MITK (www.mitk.org/) or Slicer (www.slicer.org/) to cite just two.

5. Future trends

In this paper we have shown that atlas-based segmentation has become a standard paradigm for exploiting spatial prior knowledge in MR brain image segmentation.

5.1. *Temporal and regional atlas*

We have seen that both topological and statistical atlases provide helpful information regarding brain anatomy and its variability. Using a single-subject atlas for label propagation is the most straightforward strategy, but clearly not the best to overcome anatomical variability. As presented in Section 3.2, improved segmentations are achieved with multi-atlas based techniques [63–68] where multiple individuals are selected as atlases for label propagation and their segmentation results can be fused by majority voting rule [69,70], weighted voting [68,71,72] or EM-based strategies [74,75]. However, multi-atlas segmentation strategies outperform single atlas-based segmentation methods at a much higher computational cost [156]. A different way to combine multiple atlases is to create a population-based template. Several methods have been suggested for averaging brains and registering them group-wise to avoid any bias [34–41,157].

Recently, several studies have shown that selection of the atlas, or group of atlases, is crucial for improving segmentation results [65,66], for a given pathology [32,33], for instance. It is particularly important in developing populations like newborns and infants [119,120,158,159], where age-related atlases are chosen. Thus, research interests currently focus on the construction of *temporal* (also called *4D*) atlases for developing, growing and aging populations [127,160–163]. The goal of these dynamic probabilistic atlases is twofold: to capture both inter-subject and longitudinal anatomical variability.

New atlases will aim to encode the anatomical differences locally. The importance of region-wise atlases has been shown recently by [164–166]. Such approaches aim to overcome the limitation of most current atlases, whereby all voxels in all atlases are considered equally important. Further, Shi et al. [166] claim that even better results can be obtained with multiple atlases matched according to adaptive weighting schemes.

5.2. *Combining segmentation and registration*

In Section 3, we presented atlas-based segmentation methods grouped into three different strategies: *label propagation*, *multi-atlas techniques*, and *probabilistic atlas-based segmentation*. The three strategies are registration-based, that is, they rely on the deformation of the atlas objects to match their corresponding objects in the patient image to be segmented. We believe that having such a transformation or deformation field between the atlas and the patient has one main advantage: the position of structures with fuzzy contours or without visible contours can be estimated. Consider the subthalamic nuclei targeting used in the treatment of Parkinson's disease [167,168], for instance. However, if the registration procedure relies only on intensity-based similarity measures, the segmentation obtained by applying the estimated transformation to the atlas fails to exploit other information contained in the grey-level atlas image, such as the shape or texture of the structure of interest and similar features of adjacent regions. Moreover, these strategies assume a point-to-point correspondence between atlas and subject, providing very poor segmentation results (if no special procedures are used) in cases where anatomical inconsistencies exist.

To overcome these limitations, novel atlas-based segmentation methods aim to combine segmentation and registration methods either alternatively or jointly. Iterative interleaving registration and segmentation steps have been presented for brain tissue segmentation in [108,114,169]. The idea in these works is that in one step the registration helps the segmentation and in the following step the segmentation helps the registration.

Joint registration-segmentation methods allow the inclusion of more local constraints during matching while computing a deformation field. A first group of approaches track the deformation of the atlas contours modelled by a level set function during an active contour-based segmentation process [170,171]. A second group of methods extracts the contours of the same objects within both atlas and subject images and, at the same time, compute the deformation between the contours of these objects. This idea is sug-

gested in two different frameworks: coupling active contour segmentation to registration in an energy-based variational framework [172–174] and labelling brain tissue jointly with the registration task using Markov Random Fields [175,176].

5.3. Conclusions

Many avenues remain to be investigated in the research of atlas-based segmentation for MR brain imaging. Here we have outlined two of them: combining segmentation and registration methods, and adding regional and temporal information in atlases. We believe that these new trends will improve the paradigm for exploiting spatial prior knowledge in MR imaging, obtaining faster and more robust segmentation methods which can significantly help crucial aspects of every-day clinical practice such as diagnosis, follow-up and brain mapping studies.

Conflict of interest

All authors in this paper have no potential conflict of interests.

Acknowledgements

First of all, we would like to thank Prof. Reyer Zwiggelaar from Aberystwyth University, United Kingdom, for his valuable comments and suggestions for improving the presentation of this work. We would like to thanks also the reviewers for their critical evaluation of the manuscript. Our acknowledgement also goes to the collaborators who provide us with medical images: Dr. L. Guibaud (Hôpital Femme Mére Enfant, Hospices Civils de Lyon, France), Dr. B. Draganski and Dr. E. Fornari (University Hospital Center and University of Lausanne, Switzerland), Dr. A. Rovira (Vall d'Hebron University Hospital, Spain), Dr. Ll. Ramió-Torrentà (Dr. Josep Trueta University Hospital, Spain), Dr. J.C. Vilanova (Girona Magnetic Resonance Center, Spain).

This study has been supported by the Instituto de Salud Carlos III Grant PI09/91018, and Grant VALTEC09-1-0025 from the Generalitat de Catalunya. M. Cabezas holds a FI grant 2010FI_B 00574. This study is also supported by the Center for Biomedical Imaging (CIBM) of the Geneva and Lausanne Universities and the EPFL, as well as the Leenaards and Louis Jeantet foundations.

Appendix A. Evaluation measures

A common evaluation measure for brain segmentation is the Dice similarity coefficient (DSC) [177], an overlap metric between two binary masks defined as:

$$\mathrm{DSC} = \frac{2 \cdot |A \cap M|}{|A| + |M|}, \tag{A.1}$$

where A represents the automatic segmentation mask and M the manual segmentation from the expert. DSC ranges between [0, 1], and DSC values equal or higher than 0.7 are usually considered as a good agreement between two binary masks [178].

This measure is mathematically related to the Area Overlap (A_{ov}), another common similarity index presented by Jaccard [179]. The A_{ov} also ranges between [0, 1], and it is defined as:

$$A_{ov} = \frac{|A \cap M|}{|A \cup M|}. \tag{A.2}$$

The relationship between both measures is expressed by the following equation:

$$\mathrm{DSC} = \frac{2 \cdot A_{ov}}{1 + A_{ov}}. \tag{A.3}$$

Note that values from the DSC similarity index are expected to be higher:

$$\mathrm{DSC} > A_{ov} \Rightarrow \frac{2 \cdot A_{ov}}{1 + A_{ov}} > A_{ov} \Rightarrow 2 > 1 + A_{ov}.$$

Other similarity measures used are the True Positive Rate or the Kappa statistic. However, the use of these measures is limited to few studies, the above mentioned DSC and A_{ov} being the most widely used.

Note that in this work we have translated some results presented as A_{ov} to DSC to provide a more clear comparison.

REFERENCES

[1] A. Rovira, J. Swanton, M. Tintoré, E. Huerga, F. Barkhof, M. Filippi, J.L. Frederiksen, A. Langkilde, K. Miszkiel, C. Polman, M. Rovaris, J. Sastre-Garriga, D. Miller, X. Montalban, A single, early magnetic resonance imaging study in the diagnosis of multiple sclerosis, Arch. Neurol. 66 (5) (2009) 587–592.
[2] Y. Ge, Multiple sclerosis: the role of MR imaging, Am. J. Neuroradiol. 27 (6) (2006) 1165–1176.
[3] D. Hill, Neuroimaging to assess safety and efficacy of AD therapies, Expert Opin. Investig. Drugs 19 (1) (2010) 23–26.
[4] R.E. Jung, J.M. Segall, H.J. Bockholt, R.A. Flores, S.M. Smith, R.S. Chavez, R.J. Haier, Neuroanatomy of creativity, Hum. Brain Mapp. 31 (3) (2010) 398–409.
[5] E. Angelini, Y. Jin, A. Laine, State of the art of level set methods in segmentation and registration of medical imaging modalities, in: Handbook of Biomedical Image Analysis, Springer, US, 2007, pp. 47–101.
[6] T.F. Cootes, C.J. Taylor, D.H. Cooper, J. Graham, Active shape models – their training and application, Comput. Vis. Image Underst. 61 (1) (1995) 38–59.
[7] T. Cootes, C. Beeston, G. Edwards, C. Taylor, A unified framework for atlas matching using active appearance models, in: Int. Conf. Image Proc. Med. Ima., 1999, pp. 322–333.
[8] D. Rueckert, L. Sonoda, C. Hayes, D. Hill, M. Leach, D. Hawkes, Nonrigid registration using free-form deformations: application to breast MR images, IEEE Trans. Med. Imag. 18 (8) (1999) 712–721.
[9] J.B.A. Maintz, M.A. Viergever, A survey of medical image registration, Med. Image Anal. 2 (1) (1998) 1–36.
[10] H. Lester, S.R. Arridge, A survey of hierarchical non-linear medical image registration, Pattern Recogn. 32 (1) (1999) 129–149.
[11] D.L.G. Hill, P.G. Batchelor, M. Holden, D.J. Hawkes, Medical image registration, Phys. Med. Biol. 46 (3) (2001) R1–R45.
[12] J.P.W. Pluim, J.B.A. Maintz, M.A. Viergever, Mutual-information-based registration of medical images: a survey, IEEE Trans. Med. Imag. 22 (8) (2003) 986–1004.

[13] A. Gholipour, N. Kehtarnavaz, R. Briggs, M. Devous, K. Gopinath, Brain functional localization: a survey of image registration techniques, IEEE Trans. Med. Imag. 26 (4) (2007) 427–451.
[14] J. Talairach, M. David, P. Tournoux, H. Corredor, T. Kvasina, Atlas d' Anatomie Stéréotaxique des Noyaux Gris Centraux, Masson, Paris, 1957.
[15] J. Talairach, P. Tournoux, Co-planar Stereotaxic Atlas of the Human Brain, Mark Rayport, Trans. Thieme, Stuttgart, 1988.
[16] N. Library of Medicine, The visible human project. http://www.nlm.nih.gov/research/visible/, last visit: 29/12/2010.
[17] T. Greitz, C. Bohm, S. Holte, L. Eriksson, A computerized brain atlas: construction, anatomical content and some applications, J. Comput. Assist. Tomogr. 15 (1) (1991) 26–38.
[18] L. Thurjfell, C. Bohm, T. Greitz, L. Eriksson, Transformations and algorithms in a computerized brain atlas, IEEE Trans. Nucl. Sci. 40 (4) (1993) 1187–1191.
[19] R. Kikinis, M. Shenton, D. Iosifescu, R. McCarley, P. Saiviroonporn, H. Hokama, A. Robantino, D. Metcalf, C. Wible, C. Portas, R. Donnino, F. Jolesz, A digital brain atlas for surgical planning, model driven segmentation and teaching, IEEE Trans. Visual Comput. Graph. 2 (3) (1996) 232–241.
[20] R. Bajcsy, R. Lieberson, M. Reivich, A computerized system for the elastic matching of deformed radiographic images to idealized atlas images, J. Comput. Assist. Tomogr. 7 (4) (1983) 618–625.
[21] R. Bajcsy, Digital anatomy atlas and its registration to MRI, fMRI, PET: the past presents a future, in: Int. Workshop on Biomedical Image Registration, 2003, pp. 201–211.
[22] D.L. Collins, A.P. Zijdenbos, V. Kollokian, J.G. Sled, N.J. Kabani, C.J. Holmes, A.C. Evans, Design and construction of a realistic digital brain phantom, IEEE Trans. Med. Imag. 17 (3) (1998) 463–468.
[23] M. Brain Imaging Center, BrainWeb: simulated brain database. http://www.bic.mni.mcgill.ca/brainweb/, last visit: 29/12/2010.
[24] K. Hohne, M. Bomans, M. Riemer, R. Schubert, U. Tiede, W. Lierse, A volume based anatomical atlas, IEEE Comput. Graph. Appl. 12 (4) (1992) 72–78.
[25] R. Woods, M. Dapretto, N. Sicotte, A. Toga, J. Mazziotta, Creation and use of a Tailarach-compatible atlas for accurate, automated, nonlinear intersubject registration, and analysis of functional imaging, Hum. Brain Mapp. 8 (2–3) (1999) 554–566.
[26] A. Evans, D. Collins, P. Neelin, M. Kamber, T.S. Marrett, Three-dimensional correlative imaging: applications in human brain mapping, in: Functional Neuroimaging: Technical Foundations, Academic Press, 1994, pp. 145–162.
[27] Laboratory of Neuro Imaging (UCLA), International Consortium for Brain Mapping. http://www.loni.ucla.edu/ICBM/, last visit: 29/12/2010.
[28] Laboratory of Neuro Imaging (UCLA), International Consortium for Brain Mapping. http://www.loni.ucla.edu/Atlases/, last visit: 20/03/2010.
[29] Massachusetts General Hospital, Internet Brain Segmentation Repository. http://www.cma.mgh.harvard.edu/ibsr/, last visit: 29/12/2010.
[30] N. Shiee, P.L. Bazin, A. Ozturk, D.S. Reich, P.A. Calabresi, D.L. Pham, A topology-preserving approach to the segmentation of brain images with multiple sclerosis lesions, NeuroImage 49 (2) (2010) 1524–1535.
[31] P.L. Bazin, D.L. Pham, Homeomorphic brain image segmentation with topological and statistical atlases, Med. Image Anal. 12 (5) (2008) 616–625.
[32] J.C. Mazziotta, A.W. Toga, R.S.J. Frackowiak, Brain Mapping: The Disorders, Academic Press, 2000.
[33] M.M. Esiri, J.H. Morris, The Neuropathology of Dementia, Cambridge University Press, 2002.
[34] A. Guimond, J. Meunier, J. Thirion, Average brain models: a convergence study, Comput. Vis. Image Underst. 77 (9) (2000) 192–210.
[35] M. De Craene, A. du Bois d'Aische, B. Macq, S.K. Warfield, Multi-subject registration for unbiased statistical atlas construction, in: Int. Conf. Med. Image Comput. Comput. Assist. Interv., 2004, pp. 655–662.
[36] S. Joshi, B. Davis, M. Jomier, G. Gerig, Unbiased diffeomorphic atlas construction for computational anatomy, NeuroImage 23 (1) (2004) 151–160.
[37] K.K. Bhatia, J.V. Hajnal, B.K. Puri, A. Edwards, D. Rueckert, Consistent groupwise non-rigid registration for atlas construction, in: IEEE Int. Symp. Biomed. Imag., 2003, pp. 201–211.
[38] P. Lorenzen, B. Davis, S. Joshi, Unbiased atlas formation via large deformations metric mapping, in: Int. Conf. Med. Image Comput. Comput. Assist. Interv., 2005, pp. 411–418.
[39] H. Park, P. Bland, A. Hero, C. Meyer, Least biased target selection in probabilistic atlas construction, in: Int. Conf. Med. Image Comput. Comput. Assist. Interv., 2005, pp. 419–426.
[40] L. Zollei, E.L. Miller, W. Grimson, W.M. Wells III, Efficient population registration of 3D data, Comput. Vis. Biomed. Image Appl. (2005) 291–301.
[41] O. Commowick, G. Malandain, Evaluation of atlas construction strategies in the context of radiotherapy planning, in: Statist. Atlases Personal. Models Work., 2006, pp. 1–4, held in conjuction with MICCAI.
[42] J.C. Gee, M. Reivich, R. Bajcsy, Elastically deforming 3D atlas to match anatomical brain images, J. Comput. Assist. Tomogr. 17 (2) (1993) 225–236.
[43] M.I. Miller, G.E. Christensen, Y. Amit, U. Grenander, Mathematical textbook of deformable neuroanatomies, Proc. Natl. Acad. Sci. U. S. A. 90 (24) (1993) 11944–11948.
[44] D.L. Collins, C.J. Holmes, T.M. Peters, A.C. Evans, Automatic 3D model-based neuroanatomical segmentation, Hum. Brain Mapp. 3 (3) (1995) 190–208.
[45] G.E. Christensen, R.D. Rabbitt, M.I. Miller, Deformable templates using large deformation kinematics, IEEE Trans. Image Proc. 5 (10) (1996) 1435–1447.
[46] D.V. Iosifescu, M.E. Shenton, S.K. Warfield, R. kikinis, J. Dengler, F.A. Jolesz, R.W. McCarley, An automated registration algorithm for measuring MRI subcortical brain structures, NeuroImage 6 (1) (1997) 13–25.
[47] C. Davatzikos, Spatial transformation and registration of brain images using elastically deformable models, Comput. Vis. Image Underst. 66 (2) (1997) 207–222.
[48] B.M. Dawant, S.L. Hartmann, J.P. Thirion, F. Maes, D. Vandermeulen, P. Demaerel, Automatic 3-D segmentation of internal structures of the head in MR images using a combination of similarity and free-form transformations. i. Methodology and validation on normal subjects, IEEE Trans. Med. Imag. 18 (10) (1999) 909–916.
[49] C. Baillard, P. Hellier, C. Barillot, Segmentation of brain 3D MR images using level sets and dense registration, Med. Image Anal. 5 (3) (2001) 185–194.
[50] A. Klein, J. Hirsch, Mindboggle: a scatterbrained approach to automate brain labeling, NeuroImage 24 (2) (2005) 261–280.
[51] Y. Wu, S.K. Warfield, I.L. Tan, W.M. Wells, D.S. Meier, R.A. van Schijndel, F. Barkhof, C.R.G. Guttmann III, Automated segmentation of multiple sclerosis lesion subtypes with multichannel MRI, NeuroImage 32 (3) (2006) 1205–1215.

[52] C. Ciofolo, C. Barillot, Atlas-based segmentation of 3D cerebral structures with competitive level sets and fuzzy control, Med. Image Anal. 13 (3) (2009) 456–470.
[53] P. Hellier, C. Barillot, A hierarchical parametric algorithm for deformable multimodal image registration, Comput. Meth. Prog. Biomed. 75 (2) (2004) 107–115.
[54] A. Andronache, M. von Siebenthal, G. Szekely, P. Cattin, Non-rigid registration of multi-modal images using both mutual information and cross-correlation, Med. Image Anal. 12 (1) (2008) 3–15.
[55] X. Han, B. Fischl, Atlas renormalization for improved brain MR image segmentation across scanner platforms, IEEE Trans. Med. Imag. 26 (4) (2007) 479–486.
[56] J. Ashburner, K.J. Friston, Nonlinear spatial normalization using basis functions, Hum. Brain Mapp. 7 (4) (1999) 209–217.
[57] V. Noblet, C. Heinrich, F. Heitz, J.P. Armspach, 3-D deformable image registration: a topology preservation scheme based on hierarchical deformation models and interval analysis optimization, IEEE Trans. Image Proc. 14 (5) (2005) 553–566.
[58] B.C. Vemuri, J. Ye, Y. Chen, C.M. Leonard, A level-set based approach to image registration, in: IEEE Work. Math. Meth. Biomed. Imag. Anal., 2000, pp. 86–93.
[59] J.P. Thirion, Image matching as a diffusion process: an analogy with Maxwell's demons, Med. Image Anal. 2 (3) (1998) 243–260.
[60] T. Vercauteren, X. Pennec, A. Perchant, N. Ayache, Diffeomorphic demons: efficient non-parametric image registration, NeuroImage 45 (Suppl. 1) (2009) S61–S72.
[61] B.C. Vemuri, S. Huang, S. Sahni, C.M. Leonard, C. Mohr, R. Gilmore, J. Fitzsimmons, An efficient motion estimator with application to medical image registration, Med. Image Anal. 2 (1) (1998) 79–98.
[62] G. Postelnicu, L. Zollei, B. Fischl, Combined volumetric and surface registration, IEEE Trans. Med. Imag. 28 (4) (2009) 508–522.
[63] A. Klein, B. Mensh, S. Ghosh, J. Tourville, J. Hirsch, Mindboggle: automated brain labeling with multiple atlases, BMC Med. Imag. 5 (1) (2005) 7.
[64] M. Wu, C. Rosano, P. Lopez-Garcia, C.S. Carter, H.J. Aizenstein, Optimum template selection for atlas-based segmentation, NeuroImage 34 (4) (2007) 1612–1618.
[65] P. Aljabar, R.A. Heckemann, A. Hammers, J.V. Hajnal, D. Rueckert, Multi-atlas based segmentation of brain images: atlas selection and its effect on accuracy, NeuroImage 46 (3) (2009) 726–738.
[66] J.M. Lötjönen, R. Wolz, J.R. Koikkalainen, L. Thurfjell, G. Waldemar, H. Soininen, D. Rueckert, Fast and robust multi-atlas segmentation of brain magnetic resonance images, NeuroImage 49 (3) (2010) 2352–2365.
[67] R.A. Heckemann, J.V. Hajnal, P. Aljabar, D. Rueckert, A. Hammers, Automatic anatomical brain MRI segmentation combining label propagation and decision fusion, NeuroImage 33 (1) (2006) 115–126.
[68] X. Artaechevarria, A. Muñoz-Barrutia, C. Ortiz-de Solorzano, Combination strategies in multi-atlas image segmentation: application to brain MR data, IEEE Trans. Med. Imag. 28 (8) (2009) 1266–1277.
[69] L. Xu, A. Krzyzak, C.Y. Suen, Methods of combining multiple classifiers and their applications to handwriting recognition, IEEE Trans. Syst. Man Cybern. 22 (3) (1992) 418–435.
[70] T. Rohlfing, R. Brandt, R. Menzel, C.R. Maurer Jr., Evaluation of atlas selection strategies for atlas-based image segmentation with application to confocal microscopy images of bee brains, NeuroImage 21 (4) (2004) 1428–1442.
[71] L.I. Kuncheva, Combining Pattern Classifiers: Methods and Algorithms, Wiley-Interscience, 2004.
[72] I. Isgum, M. Staring, A. Rutten, M. Prokop, M.A. Viergever, B. van Ginneken, Multi-atlas-based segmentation with local decision fusion – application to cardiac and aortic segmentation in CT scans, IEEE Trans. Med. Imag. 28 (7) (2004) 1000–1010.
[73] M.R. Sabuncu, B.T.T. Yeo, K. van Leemput, B. Fischl, P. Golland, A generative model for image segmentation based on label fusion, IEEE Trans. Med. Imag. 29 (10) (2010) 1714–1729.
[74] S.K. Warfield, K.H. Zou, W.M. Wells III, Simultaneous truth and performance level estimation (STAPLE): an algorithm for the validation of image segmentation, IEEE Trans. Med. Imag. 23 (7) (2004) 903–921.
[75] T. Rohlfing, D.B. Russakoff, C.R. Maurer Jr., Performance-based classifier combination in atlas-based image segmentation using expectation–maximization parameter estimation, IEEE Trans. Med. Imag. 23 (8) (2004) 983–994.
[76] K. Van Leemput, F. Maes, D. Vandermeulen, P. Suetens, Automated model-based tissue classification of MR images of the brain, IEEE Trans. Med. Imag. 18 (10) (1999) 897–908.
[77] K. Van Leemput, F. Maes, D. Vandermeulen, A. Colchester, P. Suetens, Automated segmentation of multiple sclerosis lesions by model outlier detection, IEEE Trans. Med. Imag. 20 (8) (2001) 677–688.
[78] B. Fischl, D.H. Salat, E. Busa, M. Albert, M. Dieterich, C. Haselgrove, A. van der Kouwe, R. Killiany, D. Kennedy, S. Klaveness, A. Montillo, N. Makris, B. Rosen, A.M. Dale, Whole brain segmentation: automated labeling of neuroanatomical structures in the human brain, Neuron 33 (3) (2002) 341–355.
[79] S.P. Awate, T. Tasdizen, N. Foster, R.T. Whitaker, Adaptive Markov modeling for mutual-information-based, unsupervised MRI brain-tissue classification, Med. Image Anal. 10 (5) (2006) 726–739.
[80] F. van der Lijn, T. den Heijer, M.M.B. Breteler, W. Niessen, Hippocampus segmentation in MR images using atlas registration, voxel classification, and graph cuts, NeuroImage 43 (4) (2008) 708–720.
[81] S. Bricq, C. Collet, J. Armspach, MS lesion segmentation based on hidden markov chains, in: Grand Challenge Work.: Mult. Scler. Lesion Segm. Challenge, 2008, pp. 1–9.
[82] S. Bricq, C. Collet, J.P. Armspach, Unifying framework for multimodal brain MRI segmentation based on Hidden Markov Chains, Med. Image Anal. 12 (6) (2008) 639–652.
[83] J.C. Souplet, C. Lebrun, N. Ayache, G. Malandain, An automatic segmentation of T2-FLAIR multiple sclerosis lesions, in: Grand Challenge Work.: Mult. Scler. Lesion Segm. Challenge, 2008, pp. 1–11.
[84] J.L. Marroquin, B.C. Vemuri, S. Botello, E. Calderón, A. Fernández-Bouzas, An accurate and efficient Bayesian method for automatic segmentation of brain MRI, IEEE Trans. Med. Imag. 21 (8) (2002) 934–945.
[85] N. Shiee, P.L. Bazin, J.L. Cuzzocreo, D.S. Reich, P.A. Calabresi, D.L. Pham, Topologically constrained segmentation of brain images with multiple sclerosis lesions, in: Work. Med. Image Anal. Mult. Scler., 2008, pp. 71–81.
[86] N. Shiee, P. Bazin, D.L. Pham, Multiple sclerosis lesion segmentation using statistical and topological atlases, in: Grand Challenge Work.: Mult. Scler. Lesion Segm. Challenge, 2008, pp. 1–10.
[87] M. Kamber, R. Shinghal, D.L. Collins, G.S. Francis, A.C. Evans, Model-based 3-D segmentation of multiple sclerosis lesions in magnetic resonance brain images, IEEE Trans. Med. Imag. 14 (3) (1995) 442–453.

[88] A.P. Zijdenbos, R. Forghani, A.C. Evans, Automatic "pipeline" analysis of 3-D MRI data for clinical trials: application to multiple sclerosis, IEEE Trans. Med. Imag. 21 (10) (2002) 1280–1291.
[89] D.J. Kroon, E. van Oort, K. Slump, Multiple sclerosis detection in multispectral magnetic resonance images with principal components analysis, in: Grand Challenge Work.: Mult. Scler. Lesion Segm. Challenge, 2008, pp. 1–14.
[90] A. Akselrod-Ballin, M. Galun, J.M. Gomori, M. Filippi, P. Valsasina, R. Basri, A. Brandt, Automatic segmentation and classification of multiple sclerosis in multichannel MRI, IEEE Trans. Biomed. Eng. 56 (10) (2009) 2461–2469.
[91] C.A. Cocosco, A.P. Zijdenbos, A.C. Evans, A fully automatic and robust brain MRI tissue classification method, Med. Image Anal. 7 (4) (2003) 513–527.
[92] H.A. Vrooman, C.A. Cocosco, F. van der Lijn, R. Stokking, M.A. Ikram, M.W. Vernooij, M.M.B. Breteler, W.J. Niessen, Multi-spectral brain tissue segmentation using automatically trained k-nearest-neighbor classification, NeuroImage 37 (1) (2007) 71–81.
[93] R. de Boer, H.A. Vrooman, F. van der Lijn, M.W. Vernooij, M.A. Ikram, A. van der Lugt, M.M.B. Breteler, W.J. Niessen, White matter lesion extension to automatic brain tissue segmentation on MRI, NeuroImage 45 (4) (2009) 1151–1161.
[94] X. Tomas, S.K. Warfield, Fully-automatic generation of training points for automatic multiple sclerosis segmentation, in: Work. Med. Image Anal. Mult. Scler., 2009, pp. 49–59.
[95] M. Prastawa, E. Bullitt, S. Ho, G. Gerig, A brain tumor segmentation framework based on outlier detection, Med. Image Anal. 8 (3) (2004) 275–283.
[96] M. Prastawa, G. Gerig, Automatic MS lesion segmentation by outlier detection and information theoretic region partitioning, in: Grand Challenge Work.: Mult. Scler. Lesion Segm. Challenge, 2008, pp. 1–8.
[97] V. Grau, A.U.J. Mewes, M. Alcaniz, R. Kikinis, S.K. Warfield, Improved watershed transform for medical image segmentation using prior information, IEEE Trans. Med. Imag. 23 (4) (2004) 447–458.
[98] P. DHaese, V. Duay, R. Li, A. du Bois dAische, T. Merchant, A. Cmelak, E. Donnelly, K. Niermann, B. Macq, B. Dawant, Automatic segmentation of brain structures for radiation therapy planning, in: Medical Imaging: Image Processing, ISCAS, SPIE, 2003, pp. 517–526.
[99] J.M. Lee, U. Yoon, S.H. Nam, J.H. Kim, I.Y. Kim, S.I. Kim, Evaluation of automated and semi-automated skull-stripping algorithms using similarity index and segmentation error, Comput. Biol. Med. 33 (6) (2003) 495–507.
[100] K. Boesen, K. Rehm, K. Schaper, S. Stoltzner, R. Woods, E. Lüders, D. Rottenberg, Quantitative comparison of four brain extraction algorithms, NeuroImage 22 (3) (2004) 1255–1261.
[101] C. Fennema-Notestine, I.B. Ozyurt, C.P. Clark, S. Morris, A. Bischoff-Grethe, M.W. Bondi, T.L. Jernigan, B. Fischl, F. Segonne, D.W. Shattuck, R.M. Leahy, D.E. Rex, A.W. Toga, K.H. Zou, G.G. Brown, Quantitative evaluation of automated skull-stripping methods applied to contemporary and legacy images: effects of diagnosis, bias correction and slice location, Hum. Brain Mapp. 27 (2) (2006) 99–113.
[102] S.W. Hartley, A.I. Scher, E.S.C. Korf, L.R. White, L.J. Launer, Analysis and validation of automated skull stripping tools: a validation study based on 296 MR images from the Honolulu Asia aging study, NeuroImage 30 (4) (2006) 1179–1186.
[103] M. Stella Atkins, B.T. Mackiewich, Fully automatic segmentation of the brain in MRI, IEEE Trans. Med. Imag. 17 (1) (1998) 98–107.
[104] F. Ségonne, A.M. Dale, E. Busa, M. Glessner, D. Salat, H.K. Hahn, B. Fischl, A hybrid approach to the skull stripping problem in MRI, NeuroImage 22 (3) (2004) 1060–1075.
[105] J. Besag, On the statistical analysis of dirty pictures, J. R. Stat. Soc. B 48 (3) (1986) 259–302.
[106] A.P. Dempster, N.M. Laird, D.B. Rubin, Maximum-likelihood from incomplete data via EM algorithm, J. R. Stat. Soc. B 39 (1) (1977) 1–38.
[107] J.C. Bezdek, Pattern Recognition with Fuzzy Objective Function Algorithms, Plenum Press, New York, 1981.
[108] K.M. Pohl, J. Fisher, W.E.L. Grimson, R. Kikinis, W.M. Wells III, A Bayesian model for joint segmentation and registration, NeuroImage 31 (1) (2006) 228–239.
[109] Northern California Institute for Research and Education (UCSF), Alzheimer's Disease Neuroimaging Initiative (ADNI). http://www.adni-info.org/, last visit: 01/03/2011.
[110] U. Vovk, F. Pernus, B. Likar, A review of methods for correction of intensity inhomogeneity in MRI, IEEE Trans. Med. Imag. 26 (3) (2007) 405–421.
[111] N.R. Pal, S.K. Pal, A review on image segmentation techniques, Pattern Recogn. 26 (9) (1993) 1277–1294.
[112] L.P. Clarke, R.P. Velthuizen, M.A. Camacho, J.J. Heine, M. Vaidyanathan, L.O. Hall, R.W. Thatcher, M.L. Silbiger, MRI segmentation: methods and applications, Magn. Reson. Imag. 13 (3) (1995) 343–368.
[113] J.S. Suri, S. Singh, L. Reden, Computer vision and pattern recognition techniques for 2-D and 3-D MR cerebral cortical segmentation (Part I): a state-of-the-art review, Pattern Anal. Appl. 5 (2002) 46–76.
[114] J. Ashburner, K.J. Friston, Unified segmentation, NeuroImage 26 (3) (2005) 839–851.
[115] S.K. Warfield, Fast k-NN classification for multichannel image data, Pattern Recogn. Lett. 17 (7) (1996) 713–721.
[116] N.I. Weisenfeld, A.U.J. Mewes, S.K. Warfield, Highly accurate segmentation of brain tissue and subcortical gray matter from newborn MRI, in: Int. Conf. Med. Image Comput. Comput. Assist. Interv., 2006, pp. 199–206.
[117] N.I. Weisenfeld, S.K. Warfield, Automatic segmentation of newborn brain MRI, NeuroImage 47 (2) (2009) 564–572.
[118] M. Prastawa, J.H. Gilmore, S. Jiang, J. Allsop, L. Perkins, L. Srinivasan, T. Hayat, S. Kumar, J. Hajnal, Automatic segmentation of MR images of the developing newborn brain, Med. Image Anal. 9 (5) (2005) 457–466.
[119] H. Xue, L. Srinivasan, S. Jiang, M. Rutherford, A. Edwards, D. Rueckert, J. Hajnala, Automatic segmentation and reconstruction of the cortex from neonatal MRI, NeuroImage 38 (3) (2007) 461–477.
[120] M. Murgasova, L. Dyet, D. Edwards, M. Rutherford, J. Hajnal, D. Rueckert, Segmentation of brain MRI in young children, Acad. radiol. 14 (11) (2007) 1350–1366.
[121] I. Claude, J.L. Daire, G. Sebag, Fetal brain MRI: segmentation and biometric analysis of the posterior fossa, IEEE Trans. Biomed. Eng. 51 (4) (2004) 617–626.
[122] P.A. Habas, K. Kim, F. Rousseau, O.A. Glenn, A.J. Barkovich, C. Studholme, Atlas-based segmentation of the germinal matrix from in utero clinical MRI of the fetal brain, in: Int. Conf. Med. Image Comput. Comput. Assist. Interv., 2008, pp. 351–358.
[123] M. Bach Cuadra, M. Schaer, A. Andre, L. Guibaud, S. Eliez, J.P. Thiran, Brain tissue segmentation of fetal MR images, in: Workshop on Image Anal. Dev. Brain, held in Int. Conf. Med. Image Comput. Comput. Assist. Interv., 2009, pp. 1–9.
[124] P.A. Habas, K. Kim, F. Rousseau, O.A. Glenn, A.J. Barkovich, C. Studholme, Atlas-based segmentation of developing tissues in the human brain with quantitative validation in young fetuses, Hum. Brain Mapp. 31 (9) (2010) 1348–1358.
[125] B. Mortamet, D. Zeng, G. Gerig, M. Prastawa, E. Bullitt, Effects of healthy aging measured by intracranial

compartment volumes using a designed MR brain database, in: Int. Conf. Med. Image Comput. Comput. Assist. Interv., 2005, pp. 383–391.
[126] C.D. Smith, H. Chebrolu, D.R. Wekstein, F.A. Schmitt, W.R. Markesbery, Age and gender effects on human brain anatomy: a voxel-based morphometric study in healthy elderly, Neurobiol. Aging 28 (7) (2007) 1075–1087.
[127] A.W. Toga, P.M. Thompson, Temporal dynamics of brain anatomy, Annu. Rev. Biomed. Eng. 5 (2003) 119–145.
[128] B. Draganski, J. Ashburner, C. Hutton, F. Kherif, R. Frackowiak, G. Helms, N. Weiskopf, Regional specificity of MRI contrast parameter changes in normal ageing revealed by voxel-based quantification (VBQ), NeuroImage 55 (4) (2011) 1423–1434.
[129] H. Lemaître, F. Crivello, B. Grassiot, A. Alpérovitch, C. Tzourio, B. Mazoyer, Age- and sex-related effects on the neuroanatomy of healthy elderly, NeuroImage 26 (3) (2005) 900–911.
[130] S.L. Hartmann, J.P. Thirion, F. Maes, D. Vandermeulen, P. Demaerel, Automatic 3-D segmentation of internal structures of the head in MR images using a combination of similarity and free-form transformations. ii. Validation on severly atrophied brains, IEEE Trans. Med. Imag. 18 (10) (1999) 917–926.
[131] L.W. de Jong, K. van der Hiele, I.M. Veer, J.J. Houwing, R.G.J. Westendorp, E.L.E.M. Bollen, P.W. de Bruin, H.A.M. Middelkoop, M.A. van Buchem, J. van der Grond, Strongly reduced volumes of putamen and thalamus in Alzheimer's disease: an MRI study, Brain 131 (12) (2008) 3277–3285.
[132] J.L. Whitwell, Voxel-based morphometry: an automated technique for assessing structural changes in the brain, J. Neurosci. 29 (31) (2009) 9661–9664.
[133] R. Wolz, R.A. Heckemann, P. Aljabar, J.V. Hajnal, A. Hammers, J. Lötjönen, D. Rueckert, Measurement of hippocampal atrophy using 4D graph-cut segmentation: application to ADNI, NeuroImage 52 (1) (2010) 109–118.
[134] L. Zhao, U. Ruotsalainen, J. Hirvonen, J. Hietala, J. Tohka, Automatic cerebral and cerebellar hemisphere segmentation in 3D MRI: adaptive disconnection algorithm, Med. Image Anal. 14 (3) (2010) 360–372.
[135] S. Shen, A.J. Szameitat, A. Sterr, Detection of infract lesions from single MRI modality using inconsistency between voxel intensity and spatial location – a 3D automatic approach, IEEE Trans. Inform. Technol. Biomed. 12 (4) (2008) 532–540.
[136] S. Shen, A.J. Szameitat, A. Sterr, An improved lesion detection approach based on similarity measurement between fuzzy intensity segmentation and spatial probability maps, Magn. Reson. Imaging 28 (2) (2010) 245–254.
[137] M.L. Seghier, A. Ramlackhansingha, A.P.L.J. Criniona, C.J. Pricea, Lesion identification using unified segmentation-normalisation models and fuzzy clustering, NeuroImage 41 (4) (2008) 1253–1266.
[138] G. Dugas-Phocion, M.A.G. Ballester, G. Malandain, C. Lebrun, N. Ayache, Improved EM-based tissue segmentation and partial volume effect quantification in multi-sequence brain MRI, in: Int. Conf. Med. Image Comput. Comput. Assist. Interv., 2004, pp. 13–18.
[139] M. Styner, J. Lee, B. Chin, M. Chin, O. Commowick, H. Tran, S. Markovic-Plese, V. Jewells, S. Warfield, Editorial: 3D segmentation in the clinic: a grand challenge II: MS lesion segmentation, in: MIDAS Journal – MICCAI 2008 Workshop, 2008, pp. 1–8.
[140] M. Bach Cuadra, M.D. Craene, V. Duay, B. Macq, C. Pollo, J.P. Thiran, Dense deformation field estimation for atlas-based segmentation of pathological MR brain images, Comput. Meth. Prog. Biomed. 84 (2–3) (2006) 66–75.
[141] E.I. Zacharaki, C.S. Hogea, D. Shen, G. Biros, C. Davatzikos, Non-diffeomorphic registration of brain tumor images by simulating tissue loss and tumor growth, NeuroImage 46 (3) (2009) 762–774.
[142] S. Kyriakou, C. Davatzikos, Nonlinear elastic registration of brain images with tumor pathology using a biomechanical model, IEEE Trans. Med. Imag. 18 (7) (1999) 580–592.
[143] B.M. Dawant, S.L. Hartmann, S. Gadamsetty, Brain atlas deformation in the presence of large space-occupying tumors, in: Int. Conf. Med. Image Comput. Comput. Assist. Interv., 1999, pp. 589–596.
[144] B.M. Dawant, S.L. Hartmann, S. Pan, S. Gadamsetty, Brain atlas deformation in the presence of small and large space-occupying tumors, Comput. Aided Surg. 7 (1) (2002) 1–10.
[145] M. Bach Cuadra, C. Pollo, A. Bardera, O. Cuisenaire, J.G. Villemure, J.P. Thiran, Atlas-based segmentation of pathological MR brain images using a model of lesion growth, IEEE Trans. Med. Imag. 23 (10) (2004) 1301–1314.
[146] C. Pollo, M. Bach Cuadra, O. Cuisenaire, J.-G. Villemure, J.P. Thiran, Segmentation of brain structures in presence of a space-occupying lesion, NeuroImage 24 (4) (2005) 990–996.
[147] W.L. Nowinski, D. Belov, Toward atlas-assisted automatic interpretation of MRI morphological brain scans in the presence of tumor, NeuroImage 12 (8) (2005) 1049–1057.
[148] S.K. Warfield, M. Kaus, F.A. Jolesz, R. Kikinis, Adaptive, template moderated, spatially varying statistical classification, Med. Image Anal. 4 (1) (2000) 43–55.
[149] D. Shen, C. Davatzikos, HAMMER: Hierarchical attribute matching mechanism for elastic registration, IEEE Trans. Med. Imag. 21 (11) (2002) 1421–1439.
[150] E.I. Zacharaki, D. Shen, S.K. Lee, C. Davatzikos, ORBIT: a multiresolution framework for deformable registration of brain tumor images, IEEE Trans. Med. Imag. 27 (8) (2008) 1003–1017.
[151] V. Duay, P.F. D'Haese, R. Li, B.M. Dawant, Non-rigid registration algorithm with spatially varying stiffness properties, in: IEEE Int. Symp. Biomed. Imag., 2004, pp. 408–411.
[152] R. Stefanescu, O. Commowick, G. Malandain, P.-Y. Bondiau, N. Ayache, X. Pennec, Non-rigid atlas to subject registration with pathologies for conformal brain radiotherapy, in: Int. Conf. Med. Image Comput. Comput. Assist. Interv., 2004, pp. 704–711.
[153] T. Liu, D. Shen, C. Davatzikos, Deformable registration of tumor-diseased brain images, in: Int. Conf. Med. Image Comput. Comput. Assist. Interv., 2004, pp. 720–728.
[154] N. Moon, E. Bullit, K. van Leemput, G. Gerig, Automatic brain and tumor segmentation, in: Int. Conf. Med. Image Comput. Comput. Assist. Interv., 2002, pp. 372–379.
[155] R. Desikan, F. Segonne, B. Fischl, B. Quinn, B. Dickerson, D. Blacker, R. Buckner, A. Dale, R. Maguire, B. Hyman, M. Albert, R. Killiany, An automated labeling system for subdividing the human cerebral cortex on MRI scans into gyral based regions of interest, NeuroImage 31 (3) (2006) 968–980.
[156] X. Han, L. Hibbard, V. Willcut, GPU-accelerated, gradient-free MI deformable registration for atlas-based MR brain image segmentation, in: Computer Vision and Pattern Recognition Workshop, 2009, pp. 141–148.
[157] K. Bhatia, J. Hajnal, A. Hammers, D. Rueckert, Similarity metrics for groupwise non-rigid registration, in: Int. Conf. Med. Image Comput. Comput. Assist. Interv., 2007, pp. 544–552.
[158] M. Wilke, V. Schmithorst, S. Holland, Normative pediatric brain data for spatial normalization and segmentation

differs from standard adult data, Magnetic Resonance in Medicine 50 (4) (2003) 749–757.
[159] M. Altaye, S.K. Holland, M. Wilke, C. Gaser, Infant brain probability templates for MRI segmentation and normalization, NeuroImage 43 (4) (2008) 721–730.
[160] A.W. Toga, P.M. Thompson, E.R. Sowell, Mapping brain maturation, Focus 4 (3) (2006) 378–390.
[161] A. Ericsson, P. Aljabar, D. Rueckert, Construction of a patient-specific atlas of the brain: application to normal aging, in: IEEE Int. Symp. Biomed. Imag., 2008, pp. 480–483.
[162] P.A. Habas, K. Kim, J.M. Corbett-Detig, F. Rousseau, O.A. Glenn, A.J. Barkovich, C. Studholme, A spatiotemporal atlas of MR intensity, tissue probability and shape of the fetal brain with application to segmentation, NeuroImage 53 (2) (2010) 460–470.
[163] M. Kuklisova-Murgasova, P. Aljabar, L. Srinivasan, S.J. Counsell, V. Doria, A. Serag, I.S. Gousias, J.P. Boardman, M.A. Rutherford, A.D. Edwards, J.V. Hajnal, D. Rueckert, A dynamic 4d probabilistic atlas of the developing brain, NeuroImage 54 (4) (2011) 2750–2763.
[164] E.M. van Rikxoort, I. Isgum, Y. Arzhaeva, M. Staring, S. Klein, M.A. Viergever, J.P. Pluim, B. van Ginneken, Adaptive local multi-atlas segmentation: Application to the heart and the caudate nucleus, Med. Image Anal. 14 (1) (2010) 39–49.
[165] R. Wolz, P. Aljabar, J.V. Hajnal, A. Hammers, D. Rueckert, Leap: learning embeddings for atlas propagation, NeuroImage 49 (2) (2010) 1316–1325.
[166] F. Shi, P.-T. Yap, Y. Fan, J.H. Gilmore, W. Lin, D. Shen, Construction of multi-region-multi-reference atlases for neonatal brain MRI segmentation, NeuroImage 51 (2) (2010) 684–693.
[167] P.-F. D'Haese, E. Cetinkaya, P. Konrad, C. Kao, B. Dawant, Computer-aided placement of deep brain stimulators: from planningto intraoperative guidance, IEEE Trans. Med. Imag. 24 (11) (2005) 1469–1478.
[168] F. Sanchez Castro, C. Pollo, R. Meuli, P. Maeder, O. Cuisenaire, M. Bach Cuadra, J. Villemure, J. Thiran, A cross validation study of deep brain stimulation targeting: from experts to atlas-based, segmentation-based and automatic registration algorithms, IEEE Trans. Med. Imag. 25 (11) (2006) 1440–1450.
[169] B. Fischl, D.H. Salat, A.J. van der Kouwe, N. Makris, F. Ségonne, B.T. Quinn, A.M. Dale, Sequence-independent segmentation of magnetic resonance images, NeuroImage 23 (Suppl. 1) (2004) S69–S84.
[170] V. Duay, X. Bresson, F.J. Sanchez Castro, C. Pollo, M. Bach Cuadra, J.-P. Thiran, An active contour-based atlas registration model for automatic subthalamic nucleus targeting on MRI: method and validation, in: Int. Conf. Med. Image Comput. Comput. Assist. Interv., 2008, pp. 980–988.
[171] B.C. Vemuri, J. Ye, Y. Chen, C.M. Leonard, Image registration via level-set motion: applications to atlas-based segmentation, Med. Image Anal. 7 (1) (2003) 1–20.
[172] A. Yezzi, L. Zollei, T. Kapur, A variational framework for joint segmentation and registration, in: Mathematical Methods in Biomedical Image Analysis, 2001. MMBIA 2001. IEEE Workshop on 2001, pp. 44–51.
[173] G. Unal, G. Slabaugh, Coupled PDES for non-rigid registration and segmentation, in: IEEE Conf. Comput. Vision Pattern Recogn., vol. 1, 2005, pp. 168–175.
[174] M. Droske, W. Ring, M. Rumpf, Mumford shah based registration: a comparison of a level set and a phase field approach, Comput. Visual. Sci. 12 (2009) 101–114.
[175] P.P. Wyatt, J. Noble, Map MRF joint segmentation and registration of medical images, Med. Image Anal. 7 (4) (2003) 539–552.
[176] C. Xiaohua, M. Brady, D. Rueckert, Simultaneous segmentation and registration for medical image, in: Int. Conf. Med. Image Comput. Comput. Assist. Interv., 2004, pp. 663–670.
[177] L.R. Dice, Measures of the amount of ecologic association between species, Ecology 26 (3) (1945) 297–302.
[178] J. Bartko, Measurement and reliability: statistical thinking considerations, Schizophr. Bull. 17 (3) (1991) 483–489.
[179] P. Jaccard, The distribution of flora in the alpine zone, New Phytol. 11 (2) (1912) 37–50.